Tampere University

Eetu Karpiola

PEROVSKITE SOLAR CELL OPTIMIZATION BY DEFECT PASSIVATION USING SMALL BIFUNCTIONAL ORGANIC MOLECULES

Master of Science Thesis
Faculty of Engineering and Natural Sciences
Examiners: Assoc. Prof. Paola Vivo
Dr. Ceylan Doyranli
August 2024

ABSTRACT

Eetu Karpiola: Perovskite solar cell optimization by defect passivation using small bifunctional organic molecules
Master of Science Thesis
Tampere University
Master's programme in Environmental Engineering
August 2024

The ongoing energy crisis in Europe is a key indicator that new sources for renewable energy are needed to secure our well-being. Non-renewable fossil fuels are running out slowly and humanity's energy consumption is increasing rapidly. Solar energy is a readily available renewable energy source and has significant potential to solve the energy crisis. Solar energy can be converted into electricity via solar cells. One of the promising semiconductors to harvest energy from light is halide perovskite. During last few years, perovskite-based solar cells have gained a lot of attention in research due to their ability to perform on comparable efficiencies to silicon solar cells, which are the main source of solar-harvested energy currently. Due to the low manufacturing costs and easy fabrication, perovskite solar cells are suitable and attractive for industrialization.

Unfortunately, perovskites are prone to defects, which decreases the performance of the whole device. To counter these defects, the light-harvesting layer can be passivated by using various methods, such as surface and bulk passivation. In this work, the role of two small bifunctional organic molecules, namely sodium thioglycolate and sodium hydroxyacetate, on the passivation of perovskite is investigated. These molecules have earlier proved to be successful as surface passivators in a *p-i-n* solar cell structure. In this work, a perovskite layer composed of $Cs_{0.05}(MA_{0.17}FA_{0.83})_{0.95}Pb(I_{0.83}Br_{0.17})_3$ is passivated with both molecules using both surface and bulk passivation strategies.

The goal of the thesis is to find out the best concentration for the passivator, the most promising passivation strategy, and the best passivating molecule within this study. The best concentration was determined by fabricating batches of solar cells for both surface and bulk passivation and determining the current-voltage (JV)-parameters under 1-Sun and indoor illumination (1000 lux, 4000 K). Based on the results of the measurements, the best concentration for surface passivation was 0.5 mg/ml in isopropyl alcohol (IPA) and for bulk passivation 2% v/v in dimethylsulfoxide (DMSO). Perovskite thin films were characterized by absorbance measurements, electron microscopy imaging, and X-ray diffraction analysis. Based on the characterization and better indoor performance compared to surface passivation, the bulk passivation method was chosen to be studied further. Under low-light intensities, the ideality factor of both bulk passivated devices was smaller than that of the reference, which indicates that the molecules decrease the trap assisted recombination. The calculated shunt resistances showcased that both passivating molecules lead to higher shunt resistances values than the reference, which again is beneficial for the performance of the device. Based on the measurements and characterization, the most effective passivation method within this study is bulk passivation, with concentration of 2% v/v and by using sodium thioglycolate.

The findings of passivation under low-light intensities prove that there is potential for passivation with small bifunctional organic molecules. For the future, longer maximum power point tracking time should be considered, to verify if passivation increases the life-expectancy of the perovskite solar cells.

Keywords: Solar energy, photovoltaic cells, indoor photovoltaics, perovskite, passivation

The originality of this thesis has been checked using the Turnitin Originality Check service.

TIIVISTELMÄ

Eetu Karpiola: Perovskiittiaurinkokennojen optimointi käyttäen bifunktionaalisia orgaanisia pienmolekyylejä passivoinnissa
Diplomityö
Tampereen yliopisto
Ympäristötekniikan DI-ohjelma
Elokuu 2024

Jatkuva energiakriisi Euroopassa on näyttänyt, että uusia uusiutuvia energianlähteitä tarvitaan turvataksemme hyvinvointimme. Uusiutumattomat fossiiliset polttoaineet vähenevät samalla, kun ihmisten energiankulutus lisääntyy. Aurinkoenergia on hyvin helposti saatavilla oleva energian lähde, jolla on valtava potentiaali ratkaista energiakriisi. Auringon valo voidaan muuntaa sähköenergiaksi aurinkokennojen avulla. Yksi lupaavimmista puolijohteista, joilla auringon valoa voidaan kerätä, on perovskiitti. Viimeisimpien vuosien aikana perovskiittiaurinkokennot ovat herättäneet paljon huomiota, johtuen niiden kyvystä muuntaa auringonvalo sähköksi vertailukelpoisin tuloksin verrattuna paljon käytettyihin piiaurinkokennoihin, jotka ovat tällä hetkellä käytetyin menetelmä aurinkoenergian keräämiseen. Johtuen perovskiittiaurinkokennojen matalista tuotantokuluista ja niiden helposta valmistuksesta, ne ovat hyvin houkuttelevia teolliseen tuotantoon.

Valitettavasti perovskiittiaurinkokennot ovat taipuvaisia sisäisiin heikkouksiin, jotka laskevat niiden suorituskykyä. Näiden heikkouksien torjumiseen voidaan käyttää useita eri passivointimenetelmiä, kuten pinta- ja massapassivointia. Tässä työssä passivointi tehdään käyttäen kahta pientä bifunktionaalista orgaanista molekyyliä, natrium tioglykolaattia ja natrium hydroksyyliasetaattia, joiden käytöstä pintapassivoinnissa on saatu lupaavia tuloksia *p-i-n* rakenteessa. Tässä työssä valoa absorboiva perovskiittikerros $Cs_{0.05}(MA_{0.17}FA_{0.83})_{0.95}Pb(I_{0.83}Br_{0.17})_3$ passivoidaan käyttäen molempia molekyylejä ja molempia passivointimenetelmiä.

Työn tarkoituksena on löytää paras konsentraatio, jossa molekyylejä voidaan käyttää, paras passivointimenetelmä ja lopulta paras molekyyli passivointiin tietylle menetelmälle. Tämä tehdään tuottamalla useita eriä perovskiittiaurinkokennoja eri passivointimenetelmillä ja mittaamalla niiden JV-parametrit simuloidussa auringonvalossa ja sisävalossa (1000 lux, 4000 K). Näiden tulosten perusteella paras konsentraatio pintapassivoinnille on 0.5 mg/ml isopropanolissa (IPA) ja massapassivoinnille 2 % v/v dimetyylisulfoksidissa (DMSO). Perovskiittifilmit karakterisoitiin absorptiomittausten, pyyhkäisyelektronimikroskopian ja röntgendiffraktion avulla. Massapassivoidut näytteet suoriutuvat paremmin sisävalomittauksissa kuin pintapassivoidut näytteet, jonka vuoksi massapassivointimenetelmä valittiin jatkotutkimuksiin. Alhaisen valon intensiteettimittauksissa ideaalisuuskerroin oli molemmille passivoiduille näytteille pienempi kuin referenssinäytteen, joka indikoi, että molekyylit vähentävät ansojen avustamaa rekombinaatiota. Kaikille laitteille laskettiin sunttivastukset, jotka olivat molemmilla passivoiduilla näytteillä suuremmat kuin referenssinäytteellä, mikä parantaa laitteen toimintatehokkuutta. Mittausten ja karakterisoinnin perusteella paras passivointimenetelmä on massapassivointi 2 % v/v konsentraatiolla käyttäen natrium tioglykolaattia.

Löydökset passivoinnin toimivuudesta alhaisessa valon intensiteetissä osoittaa, että bifunktionaalisilla orgaanisilla pienmolekyyleillä on potentiaalia perovskiittiaurinkokennojen passivoinnissa. Tulevaisuudessa, maksimaalisin tehopisteen seuranta-aikaa pitää pidentää, jotta nähdään parantaako passivointi perovskiittiaurinkokennojen elinajanodotetta.

Avainsanat: Aurinkoenergia, perovskiitti, passivointi

PREFACE

This thesis was carried out at Tampere University in the Hybrid Solar Cells research group. I want to thank my supervisor Associate Professor Paola Vivo for giving me a possibility to work in her group in a very interesting project. Also, for her guidance and assistance throughout the work and writing. I also want to thank my second supervisor Postdoctoral Researcher Ceylan Doyranli for teaching me everything needed to excel in perovskite solar cell fabrication, data-analysis and guidance throughout the work.

I want to thank the whole research group for being supportive and easy to work with throughout the project. Too many people to name individually as everyone has been involved with my thesis work in one way or another. Having an atmosphere where the team works toward a common goal, has casual conversations about the topics surrounding the thesis and helps each other when one is in need, is something that should not be taken granted.

Finally, I am grateful for all the support I've got from my family and friends. Last, but not least I want to thank my partner Elisa, who has been amazingly supportive and helpful during the times when the writing process hasn't been straightforward. With her assistance and read-throughs, I could overcome issues when I was stuck or feeling lost within the process.

This thesis work was supported by the SPOT-IT project, founded by the CETPartnership, the Clean and Energy Transition Partnership under the 2022 CETPartnership joint call for research proposal, co-founded by the European Commission (GA n°101069750) and Business Finland.

Tampere, 30th August 2024

Eetu Karpiola

CONTENTS

LIST OF SYMBOLS AND ABBREVIATIONS

λ	wavelength
c	speed of light
c-TiO_2	compact titanium dioxide
CB	chlorobenzene
DMF	N,N-dimethylformamide
DMSO	dimethyl sulfoxide
E	energy
E_b	binding energy
E_G	band gap
eV	electron volt
EQE	external quantum efficiency
ETL	electron transport layer
FA^+	formamidinium-ion
FF	fill factor
FK290	tris(2-(1H-pyrazol-1-yl)-4-tert-butylpyridine)cobalt(III)-tris[bis(trifuoromethylsulfonyl)imide]
FTO	fluorine-doped tin oxide
h	Planck's constant
HTL	hole transport layer
IPA	Isopropyl alcohol
IPV	Indoor photovoltaic
J_{SC}	short-circuit current density
k	Boltzmann's constant
Li-TFSI	bis(trifuoromethane)sulfonimide lithium salt
MA^+	methylammonium-ion
mp-TiO_2	mesoporous titanium dioxide
MPPT	maximum power point tracking
n_{ID}	ideality factor
n-i-p	regular device structure
P_{in}	power input to the cell
p-i-n	inverted device structure
PCE	power conversion efficiency
PL	photoluminescence
P_{out}	power output of the cell

q	elementary charge
SEM	scanning electron microscopy
Spiro-OMeTAD	2,2',7,7'-tetrakis(N,N-di-p-methoxyphenylamino)-9,9'-spiro-bifuorene
SPO	stable power output
SRH	Shockley-Read-Hall recombination
T	temperature
tBP	4-tertbutylpyridine
UV-Vis	ultraviolet-visible
V_{OC}	open-circuit voltage
XPS	X-ray photoelectron spectroscopy
XRD	X-ray diffraction

1. INTRODUCTION

During 2024, Europe has faced a significantly intensified energy, climate, and economic crises due to the Russian war in Ukraine. This has affected the energy security and left the citizens to struggle with high electricity prices. The EU installed a record 41.4 GW of solar capacity in 2022, which represented a 50% market growth from the year before. The European Commission has approved a new emergency regulation to accelerate the use of renewable energy in Europe. This new regulation is set to apply until the 30th of June 2024. Solar energy is a real solution for all the aforementioned crises. [26]

Sun is a source of clean, environmentally friendly, and freely available renewable energy on our planet. Solar energy is used to produce electricity and thermal energy. Old reliable fossil fuels are depleting on a continuous rate; therefore, it is essential to look at the sun as a source of energy. In recent years, there has been rapid development with photovoltaic materials. [30] Silicon is still the most used semiconductor in solar cells. [22]

Silicon-based solar cells are quite expensive to manufacture, rigid, and have a theoretical efficiency limit at around 29%. Perovskite solar cells have gotten increasing attention due to low-cost easy manufacturing, tunable band gap, high applicability, flexibility, high efficiency, sustainability, and potential recyclability. Perovskite solar cells, when coupled with silicon in a tandem architecture, have already exceeded 30% efficiency in laboratory conditions. Perovskite solar cells are also suitable for indoor applications due to the absorption range. [16] However, imperfections within the perovskite layer need optimization. Passivation is a way to counter the defects that are caused by fabrication process. Defects in the perovskite cause non-radiative recombination, which in turn decreases the overall performance of the photovoltaic device. [5]

In this thesis, a lead-based perovskite material $Cs_{0.05}(MA_{0.17}FA_{0.83})_{0.95}Pb(I_{0.83}Br_{0.17})_3$ by Saliba et al. is used to study the effects of surface and bulk passivation with two bifunctional small organic molecules, namely sodium thioglycolate and sodium hydroxyacetate. [24] The use of these molecules has been reported in 2023 in a *p*-*i*-*n* structure and this thesis aims to study the effects in *n*-*i*-*p* structure using surface and bulk passivation. The use of bifunctional molecules has potential to counter multiple different defects simultaneously. The first goal of the thesis is to find out the most suitable concentration for both molecules. Second goal is to determine the most effective passivation strategy between surface and bulk passivation. Third goal is to find out the best passivating molecule between sodium thioglycolate and sodium hydroxyacetate. Through these three goals, this thesis aims to identify the most optimal combination for passivation of perovskite material within set parameters. Concentration and the strategy for passivation are determined by studying the photovoltaic parameters under 1-Sun and indoor illumination (1000 lux, 4000 K) conditions. The passivation strategies are then further characterized by studying absorbance, scanning electron imaging (SEM), X-ray diffraction (XRD), stress resistance with maximum power point tracking (MPPT), and light intensity dependence to understand the passivation even further. [32]

The second chapter covers the theoretical background for the thesis by explaining the basic principles of photovoltaic cells, the structure and properties of perovskite, passivation and solar cell performance testing and film characterization needed to understand the experiments. The third chapter explains the sample preparation and solar cell fabrication methods and measurement procedures. In the fourth chapter, the results are presented, discussed and compared to other studies related to passivation. Finally, the fifth chapter is a summary of the results and summarizes the conclusions of the research work.

2. THEORY

Next, a theoretical background for the topic of the thesis is covered. In the first section, the basics of solar cell functions are discussed. The second section covers the properties and functions of a perovskite solar cell. The third section discusses the different perovskite solar cell passivation approaches. Finally, the last section focuses on solar cell performance characterization and evaluation.

2.1 Introduction to photovoltaic cells

Photovoltaics convert light into direct current when semiconductors are illuminated by photons. Semiconductors can absorb the light photons and transform a part of their energy into carriers of electrical current, namely electrons and holes. A semiconductor diode can collect and separate the carriers, and the generated current is conducted into a specific direction. A photovoltaic cell is essentially a simple semiconductor diode designed to efficiently absorb the light and convert it into electricity. [12] The energy of a photon can be expressed with an equation $E = hv$, where h is Planck's constant, and v is the speed of light. Solar spectrum comprises wavelengths from 280 nm to 4000 nm. The total irradiation on earth surface depends on the distance through atmosphere. For solar cell applications, a standardized spectrum AM1.5G is used. This corresponds to the radiation arriving to the earth's surface after passing a standard air mass 1.5 times with the solar zenith angle at 48.2°. Graph of spectral irradiance is presented in Figure 1. [3]

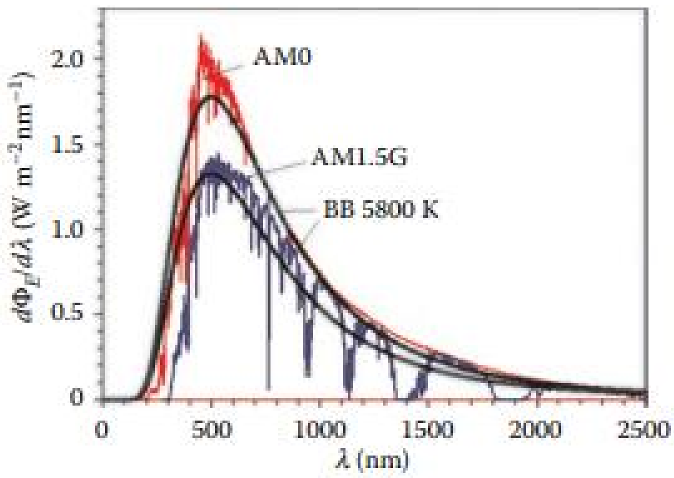

Figure 1. *A graph of the spectral irradiance, where $\frac{d\Phi}{d\lambda}$ is the energy current density per wavelength interval against the wavelength λ of the light on a solar spectrum. AM0 is the spectral irradiance from the sun outside the atmosphere, AM1.5G is the standardized spectral irradiance and BB 5800 is the spectral irradiance of a black body at 5800 K. [3]*

For the solar cell device depicted in Figure 2, the *n*-type layer is an electron deficient layer, that acts as an electron transport layer. The *p*-type layer is electron rich layer, which acts as a hole transport layer. The layers are connected via metallurgical connection. The differently charged layers create a zone between the layers, where the sunlight's photons can excite the electrons if the energy of the photon is bigger than the band gap of the semiconductor. The band gap (E_g) is an energy threshold, when exceeded the weakly bonded valence electron will move into the conduction band, where the electron can conduct electricity. The amount of energy needed to move the electron is measured in electron volts *eV.* After the current has been extracted, the electron will return to a lower energy state valence band. Photons with less energy than the band gap can't excite the electrons, and the energy carried by the photon will turn into heat inside the device. [12]

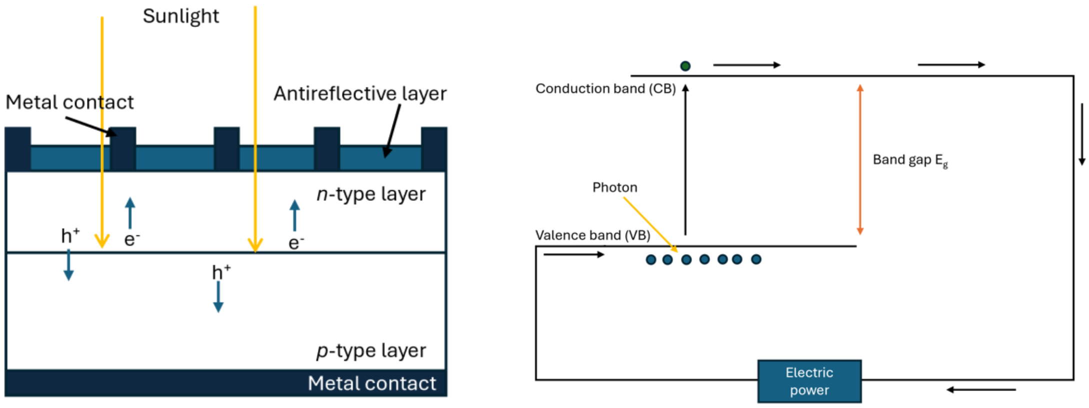

Figure 2. *Two schematic representations of a solar cell. On the left showcasing the functions of a solar cell and on the right a display of an electron excitation. [12]*

2.2 Perovskite solar cell

Perovskite is a family of substances with an ABX_3 chemical structure, which stems from that of calcium titanate ($CaTiO_3$) mineral. In the ABX_3 composition, A and B are cations and X is an anion. For perovskite, A is usually methylammonium CH_3NH^+/MA^+ or formamidinium $CH(NH_2)_2^+$/FA^+ and it occupies the vertex of the cubic lattice. Metal cations, such as Pb^{2+}, occupy the centre and then halogen anions X such as Cl^-, Br^- or I^- occupy the apex of the structure. [2] The ABX_3 structure is shown in Figure 3.

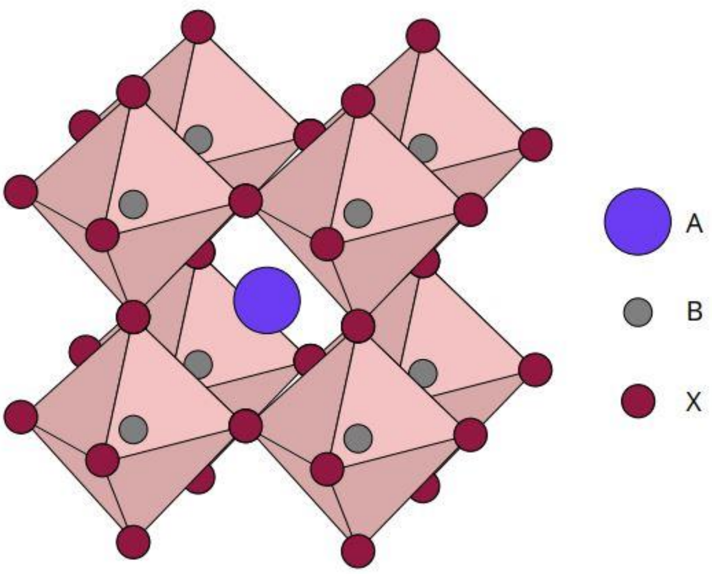

Figure 3. *The ABX_3 structure. Reprinted with permission from [21]*

The perovskite solar cell has a sandwich-like structure. The perovskite layer is deposited between two charge carrier layers: electron transport layer (ETL) and hole transport layer (HTL). Perovskite layer absorbs the light and converts the photon energy into an electron-hole pair. Excited electron moves from the valence band to the conduction band, producing current. Against other solar cell materials perovskite materials have numerous advantages like a higher absorption coefficient, longer diffusion length, a higher degree of defect tolerance and a lower rate of recombination. [1] A perovskite solar cell consists of five fundamental layers, which are the conducting substrate, hole transport layer, the light absorbing perovskite layer, electron transport layer, and a metal electrode. When the cell is illuminated, the perovskite layer creates electron-hole pairs. The ETL transports electrons to the cathode and blocks the movement of holes. Conversely, the HTL transports the holes to the anode and blocks the movement of electrons, [2] as shown schematically in Figure 4. [18]

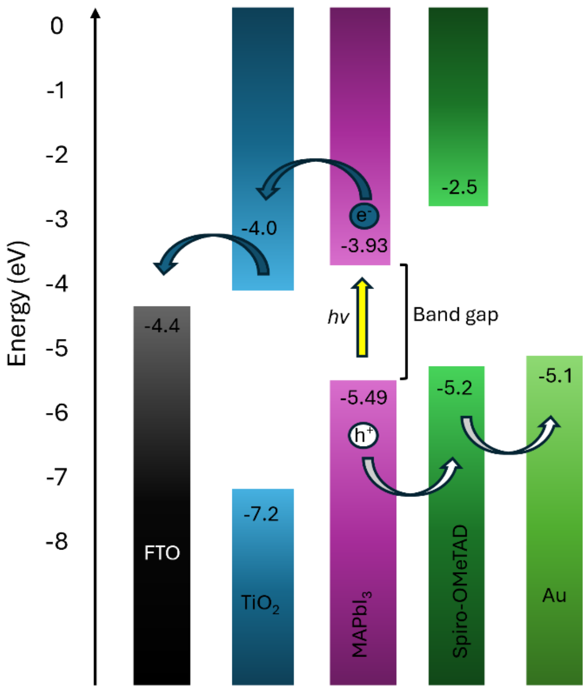

Figure 4. *Energy diagram of a perovskite solar cell. $MAPbI_2$ is being used as a perovskite layer. [18]*

The versatility of the perovskite-based device architecture and the possibility to extensively engineer is among the main reasons driving the evolution of perovskite solar cells in the early stages of the development. [28] There are three main structures for perovskite solar cells, namely planar and mesoscopic *n-i-p* and planar *p-i-n*. In the *n-i-p* structure, c-TiO_2 works as an n-type ETL and spiro-OMeTAD (2,2',7,7'-Tetrakis[N,N-di(4-methoxyphenyl)amino]-9,9'-spirobifluorene) is used a p-type HTL. The *n-i-p* device structure consists of FTO/ETL/perovskite/HTL/metal junction. For the mesoscopic *n-i-p* structure, the structure is essentially the same as the planar counterpart, but on top of the ETL there is a mesoscopic structure, usually m-TiO_2, to enhance the charge extraction. [18] The three different perovskite solar cell structures are presented in Figure 5.

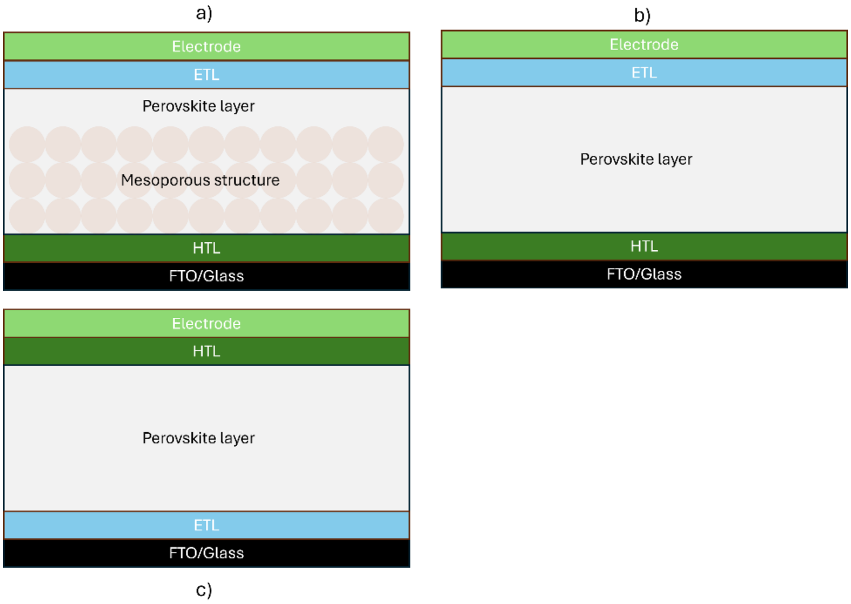

Figure 5. *Different perovskite solar cell structures: a) mesoporous n-i-p, b) planar n-i-p and c) planar p-i-n. [28].*

The complete mesoscopic structure is FTO/ETL/mesoscopic structure/perovskite/HTL/metal. The inverted *p-i-n* structure has the ETL and HTL on the opposite sides of the perovskite compared to the *n-i-p* structures. The *p-i-n* structure is FTO/HTL/perovskite/ETL/metal junction. [18] The hole transport layer in this work consists of Spiro-OMeTAD, whose structure is presented in Figure 6.

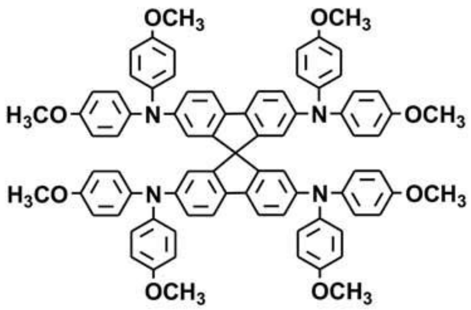

Figure 6. *The molecular structure of Spiro-OMeTAD (2,2',7,7'-Tetrakis[N,N-di(4-methoxyphenyl)amino]-9,9'-spirobifluorene) HTL. [20]*

There are multiple different ways to fabricate a perovskite solar cell. Most of the fabrication methods for silicon solar cells are expensive and need special environments compared to perovskite solar cells that can be fabricated with wet chemistry methods. [28] Fabrication techniques such as spin coating, doctor blading, screen sprinting, slot-die coating, spray coating, and inkjet printing are all usable for creating uniform layers for perovskite solar cells. In this chapter, spin coating and spray coating are further presented as these techniques are used in this work. Spin coating is a very versatile and cost-effective method for uniform deposition. Usually it is used for small-area solar cells. In the technique a solution is pipetted on to a spinning substrate. The solution will then evenly spread on the substrate due to the spinning effect. Usually after the step the substrate will be annealed to produce a high-quality uniform layer by improving the crystallization. Issues with spin coating are the significant material waste and the poor scalability of the technique. [1] Spin-coating as a method is beneficial to obtain uniform layers with great reproducibility. [34] Perovskite layer consists of grains with different sizes. Grain boundaries exist between the grains. Having a uniform perovskite layer is essential for the performance of the solar cell. Having small-sized perovskite grains, or in other words many grain boundaries, will be deleterious for the performance as it can produce short circuits. [3] This is illustrated in Figure 7.

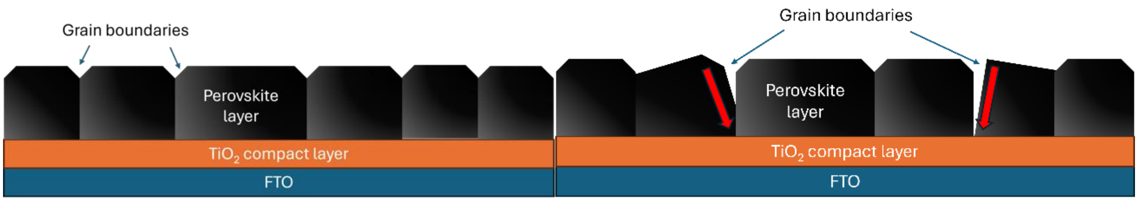

Figure 7. *On the left, an ideal uniform perovskite layer; on the right, a layer with gaps in the grain boundaries that can produce short circuits, marked with red arrows. Adapted from [3]*

Problems with the perovskite layer can be assessed with the modifications of the annealing temperatures to improve crystallization and the size of the grains and therefore decreasing the amount of grain boundaries. [3] Having less grain boundaries is beneficial for the performance of the perovskite solar cell as the number of points for short circuits are decreased and therefore the amount of non-radiative recombination is lessened. [18]

For spray coating, the solution is spread on to the substrate with the use of a carrier gas. This results in a continuous evenly spread uniform film. With the technique, the pressure of the spray, the concentration of the solution, and the distance between the nozzle and the substrate can be modified to influence the quality of the film. Issues with this technique come down to human error as the angle of the spray gun or the distance varies between the user so the film quality can be altered substantially. [1]

2.3 Passivation

Major issues with lead-based perovskite solar cells are environmental toxicity, limited stability against temperature, humidity, light exposure, and hysteresis, which is the difference between the scan directions of the JV-scans. [36] For solar cell devices there are three principal recombination methods - band-to-band, recombination with defect levels, and Auger. In band-to-band recombination, an electron makes a transition from conduction band to a low-level valence band. The energy is released with photon emission. The process is called radiative recombination. Recombination with defect levels can happen in the surface or bulk in a semiconductor. This means that the electron releases energy when transitioning from the conduction band, but it doesn't return to the valence band as it gets trapped on a level in between the bandgap. This process is called nonradiative recombination, which means that when the electron is transitioning from the conduction band to valence band, instead of photons, phonons are released that will not cause the desired effect, but instead lower the light generation efficiency and increase heat losses. Auger recombination method occurs when the conduction band electron is transitioning back to the valence band but combines with a hole between the band gap. This will cause the energy of a carrier to be relaxed to band edge energy. Therefore, this is also a nonradiative recombination method. [3] Surface and interfacial trap states cause the V_{OC} of a perovskite solar cell to decrease. These trap states also cause the perovskite solar cell to degrade. [32]

For perovskite solar cell to perform at the best possible level, the density of the charge carrier traps must be low in the grain boundaries and in the interfaces between the perovskite and charge carrier layers. This can be engineered by using passivation methods that can clear out possible traps by for example filling a vacancy on the perovskite structure or free-floating ions. [36] A schematic of the passivation is shown in Figure 8.

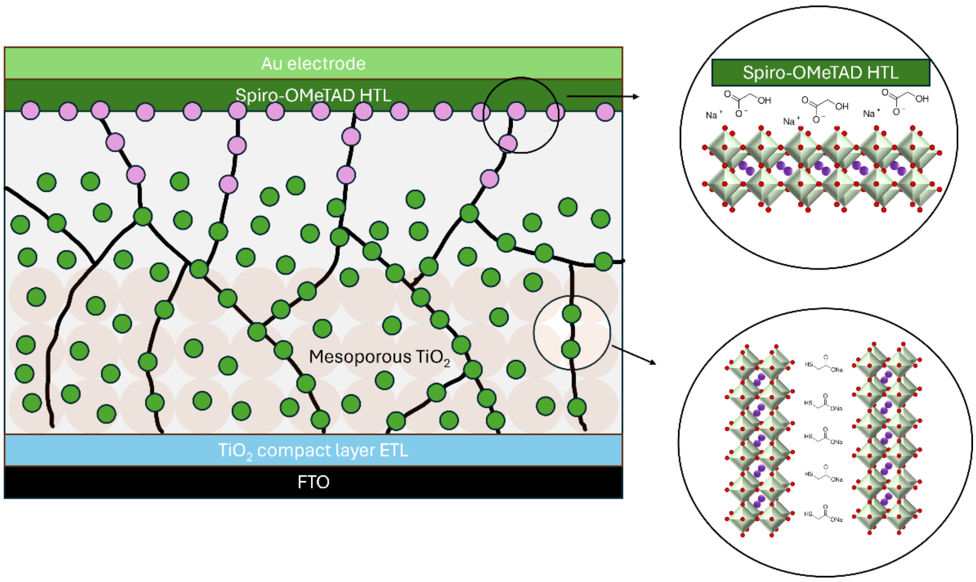

Figure 8. *Schematic of the passivation strategies. Bulk passivation is illustrated with green dots and surface passivation with purple dots. Adapted from [34]*

Bulk passivating molecules are added into the perovskite precursor and therefore the passivating molecules will be spread all out the perovskite layer. Surface passivation is done on top of the already annealed perovskite layers so the surface passivating molecules will be mainly on top of the layer but also within the most superficial grain boundaries. [34]

Passivation in perovskite solar cells can be performed in many ways. There are multiple different types of passivation methods and usually the methods aim to “fixing” a certain defect. [10] Pseudo-halides are molecules with two different functional groups. Xu et al. reported bifunctional ligands containing electron-rich functional head groups and chalcogen- or halogen-containing electron-poor functional tail groups. To prevent the production of unwanted deep impurity states that contribute to the non-radiative recombination, the chosen molecules for the machine-learning screening have a high binding energy of E_b > 3 eV. The 24 chosen molecules for the screening did not produce localized states near the band edges. After multiple rounds of screening, the best-chosen molecule was sodium thioglycolate and sodium hydroxyacetate shown in Figure 9.

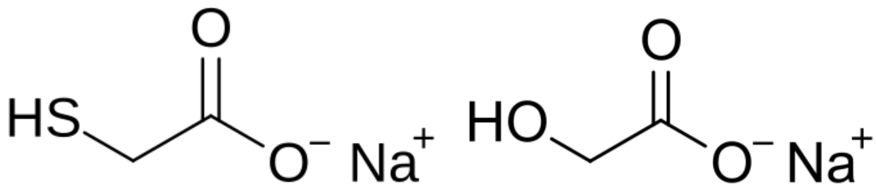

Figure 9. *Sodium thioglycolate and sodium hydroxyacetate.*

Xu et al. used five of the most promising molecules based on the screening to study the effect of the pseudo-halogen surface passivation treatment to the performance of the photovoltaic device. Also, characterization via external quantum efficiency (EQE), scanning electron microscopy (SEM), X-ray photoelectron spectroscopy (XPS), photoluminescence (PL) and X-ray diffraction (XRD) was concluded. Both molecules share a similar chemical structure having a CO^{2-}-group on head-side and HS- and OH-groups on the tail-side respectively. Together the different sides are designed to fill in donor-like defects and passivate acceptor-like defects. [32]

Within these molecules, the different passivating mechanisms included passivation with metal ion sodium (Na^+), electron donor carbonyl group (-C=O), and electron donor thiol (-SH). For Na^+-ion, the target defect is methylammonium MA^+ vacancies and undercoordinated I^-. For carbonyl group and the thiol group, the target defect is uncoordinated Pb^{2+}. [10] A schematic of different defects within the perovskite the passivation methods are designed to counter are shown in Figure 10.

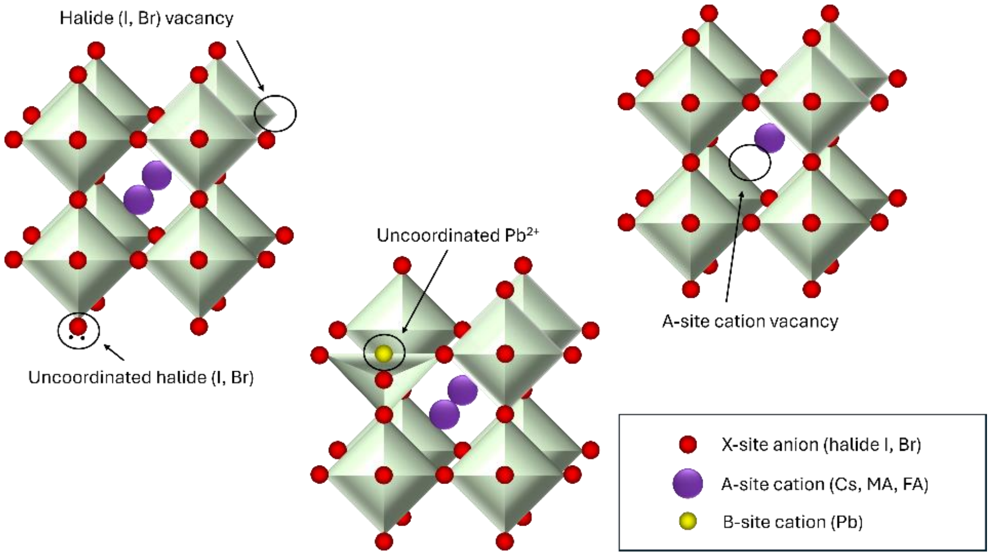

Figure 10. *Different defects with perovskite structures. Adapted from [11]*

2.4 Solar cell performance and characterization

Solar cell is designed to serve as a power supply unit. A central feature of a solar cell is its ability to create electrical power from the available radiation level. The ability is described as power conversion efficiency (*PCE*). [3] The solar cell performance can be evaluated from a current density-voltage curve called J-V-curve, that considers the photovoltage, photocurrent, and the fill factor. The fill factor depends on the shape of the J-V curve. Having a high fill factor means that the drop in the current at high voltage is delayed and therefore electrons can be extracted in the high voltage while the current is close to the short-circuit current (J_{SC}). The expression for power conversion efficiency *PCE* is shown in the equation 2.1.

$$\eta_{PCE} = \frac{P_{out}}{P_{in}} = \frac{J_{SC} \times FF \times V_{OC}}{P_{in}} \tag{2.1}$$

where J_{SC} is the short circuit current, *FF* the fill factor, V_{OC} open-circuit voltage, P_{out} the power output, and P_{in} the power of the illuminating source. [29]

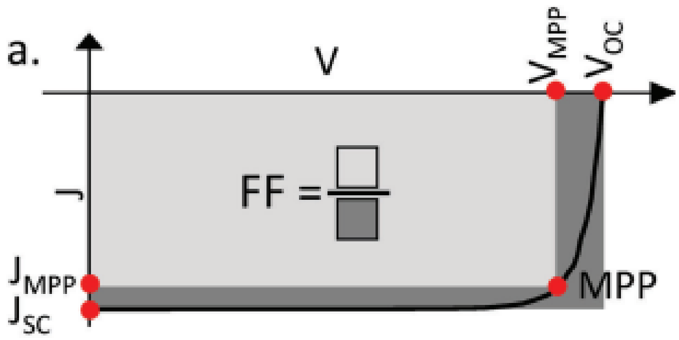

Figure 11. *The J-V curve. [29]*

In Figure 11, a typical J-V curve is depicted. *FF* is the ratio between the two different areas that are separated by the maximum power point (MPP) and the curve. In an ideal situation, the J_{SC} and J_{MPP} should match and so should the V_{OC} and the V_{MPP} to obtain an *FF* of 1. [29]

A dark J-V characteristics can be helpful for obtaining more complementary data of the recombination and the resistances of the solar device. [7] The ideality factor n_{ID} provides information of the dominating recombination methods within the devices. Usually, the ideality factor is determined by deriving it from the dark J-V curve or it can be calculated from the slope of V_{OC} *vs. ln(P)* plot if the measurements are performed with multiple different light intensities. The most common interpretation for ideality factor is that n_{ID} of 1 indicates a bimolecular process, which essentially means that the recombination rate is proportional to the product of photogenerated electron and hole densities. Ideality factor of 2 indicates Shockley-Read-Hall defect-assisted recombination (SRH). Therefore, seeing a decrease in ideality factor can be interpreted as a beneficial process for the device performance when doing passivation. [18] Series resistance in a solar cell can be caused by three different scenarios, which are the current flowing through the base and the emitter of the solar cell, the contact resistance between the metal and the transporting layer or the resistance of the metal electrodes at the top or bottom. These cause decrease in fill factor and the short-circuit current. Shunt resistance is usually caused by manufacturing defects. Low shunt resistance is a reason for power losses in the solar cell by creating alternative paths for light-generated current. This will cause a decrease in the amount of current that flows through the solar cell and therefore decreasing the performance. The shunt resistances have a bigger impact under low-light intensities as there will be less light-generated current. [9] Both of resistances are presented in Figure 12.

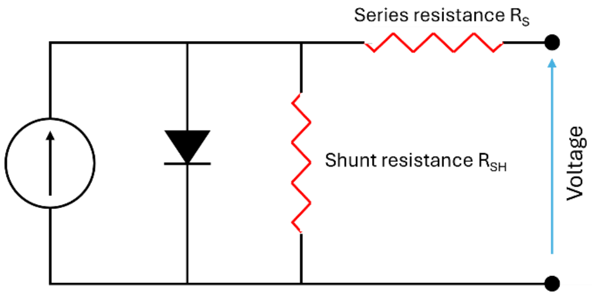

Figure 12. *A circuit diagram of series and shunt resistance in a solar cell. Adapted from [9].*

The perovskite solar cells can be also studied under indoor lighting. The technique involved with indoor devices has gained a lot of interest during recent years due to many different applications that could impact the daily human life. [27] Use of indoor photovoltaics could be beneficial for future needs of different networks of devices that are used to monitor the surroundings. As the technology progresses, the energy needed to power the sensors decrease, therefore creating possibilities for indoor photovoltaics to thrive and be used in new business opportunities. [15]

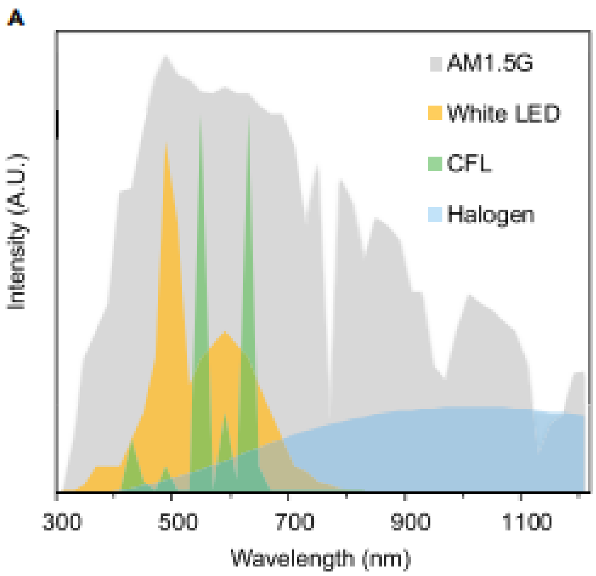

Figure 13. *Different light spectra showcasing the difference between the standard solar spectrum AM1.5G and artificial sources. [15]*

As shown in Figure 13, the spectra for indoor lighting sources are within the standard AM1.5G solar spectrum, meaning that perovskite solar cells can be used for both applications. [15] Perovskite solar cells are amazing candidates for indoor photovoltaics due to the ability to tune the band gap to exactly match the spectra of indoor illumination. [8] In 2021 Dong et al. published a paper with indoor PCE over 40%, showcasing the enormous potential that indoor photovoltaics (IPV) have yet to offer. [6]

For indoor photovoltaic measurements there are still some reliability issues with the characterization due to the differences between laboratory protocols and the lack of device characterization standards. In 2017, Chen et al. studied the performance characterization of dye-sensitized photovoltaics under indoor lighting in 15 different laboratories and compared the photovoltaic parameters of the samples obtained from all the experiments. In conclusion of the study, a substantial amount of variation in photovoltaic parameters was detected between different laboratories. Therefore, to study the IPV's the research facilities must come up with standardized protocols and measurement techniques to study and compare the cells. [4]

Perovskite solar cell can be characterized with several different methods. In this work X-ray diffraction, scanning electron microscopy and absorbance will be used to analyse the effects of passivation. Perovskite layer structure is crucial for understanding the effects of bulk passivation to the crystal lattice and therefore performance. The crystal structure can be studied with X-ray diffraction techniques. Passivation can cause micro strains in the crystal structure, which can be seen as fluctuations in the lattice spacing. This can be perceived by analysing the peak widths against the passivation-free reference sample. With this technique, both tensile and compressive strains can be noticed as both are deleterious for the performance. [35] Scanning electron microscopy is an essential method of acquiring high resolution images of the perovskite layer surface or from the cross-section of the device. In this work scanning electron microscopy will be used to study the effect of passivation to the grain size and uniformity of the perovskite layer. [2]

The band gap for perovskite can be calculated from the absorbance spectrum. Band gap is calculated with the equation 2.2

$$E_{band\ gap} = \frac{hc}{\lambda} \tag{2.2}$$

where $E_{band\ gap}$ is the band gap of the perovskite material, h is the Planck's constant, c is the speed of light and λ is the wavelength at the intersection of the fitted lines. The essential idea for the determination is presented in Figure 14. [3]

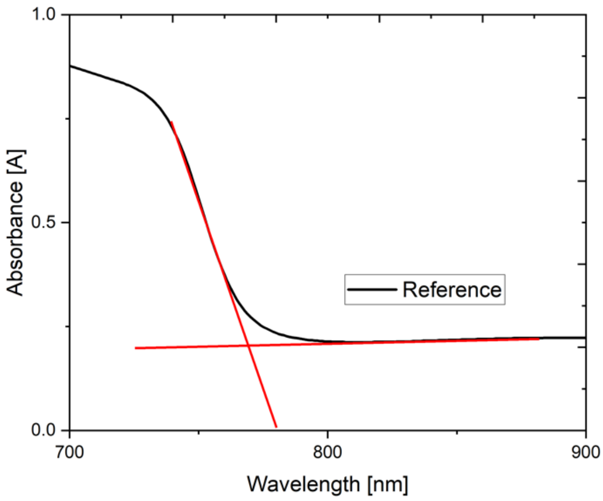

Figure 14. *How to determine the band gap from the perovskite absorption spectrum.*

3. MATERIALS AND METHODS

The experimental methods of the work are presented in this chapter. The first section describes the perovskite precursor and the preparation of the passivating solution. In the second section, the workflow for solar cell fabrication is explained. The third section includes the outdoor and indoor photovoltaic characterization and external quantum efficiency (EQE). In the fourth and concluding section of the thesis, different characterization methods are discussed, such as the X-ray diffraction (XRD), scanning electron microscopy (SEM), and absorption spectroscopy (UV-Vis). The workflow is presented in Figure 15.

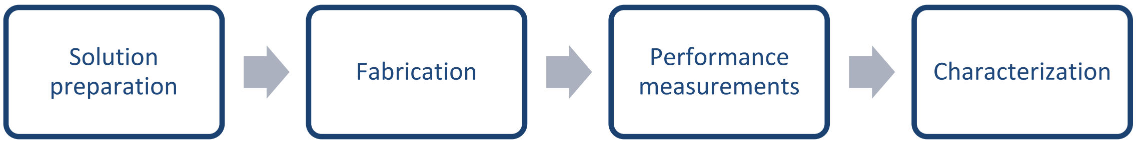

Figure 15. *A schematic of the workflow for a single device batch.*

3.1 Materials

The perovskite precursor solution is prepared according to an article by Saliba et al. (2016). For the perovskite composition of $Cs_{0.05}(MA_{0.17}FA_{0.83})_{0.95}Pb(I_{0.83}Br_{0.17})_3$, first formamidinium iodide (FAI) (0.95 M), methyl ammonium bromide (MABr) (0.19 M), lead bromide ($PbBr_2$) (0.20 M), and lead iodide (PbI_2) (1.1 M) are scaled into a vial. Then, the solids are dissolved into a 1:4 ratio of DMSO:DMF and kept stirring on a magnetic stir pad. After all the solids have dissolved, 40 µl of premade cesium iodide in DMSO (1.5M) is pipetted into the precursor solution. Then, the solution is kept under stirring without heating for 24 to 48 hours. Formamidinium iodide (FAI) and methyl ammonium bromide (MABr) were purchased from Greatcell Solar Materials. Lead bromide ($PbBr_2$, purity ≥ 98%) and lead iodide (PbI_2, purity ≥ 98%) were purchased from TCI. Cesium iodide (CsI) was obtained from abcr GmbH.

In this work, two methods for passivation are used - surface and bulk passivation. Both methods require their own solutions as the surface passivation is performed on top of the already annealed perovskite layer and the bulk passivation solution is added directly into the perovskite precursor.

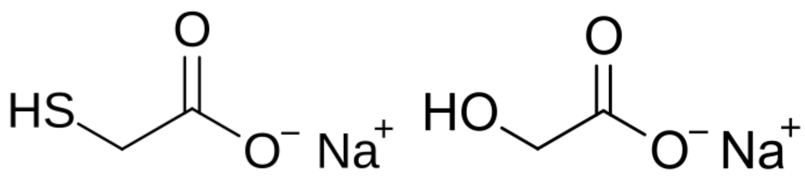

Figure 16. *Sodium thioglycolate (STG) on the left and sodium hydroxyacetate (SHA) on the right.*

For surface passivation, both molecules, sodium thioglycolate (STG) and sodium hydroxyacetate (SHA) shown in Figure 16, are dissolved into isopropyl alcohol (IPA). For the work, 1.0 mg/ml solution is prepared and let to stir on a hotplate in around 60 °C overnight. The next day the solution is filtered with a 0.22 μm filter. After filtration, the solution is diluted into working solutions, which are 0.5 mg/ml or 0.25 mg/ml, in isopropyl alcohol before deposition.

For bulk passivation, the solution is prepared similarly, but the used solvent was dimethyl sulfoxide (DMSO). First the solute is scaled and dissolved into DMSO to obtain a solution with the concentration of 0.5 mg/ml. This part was straightforward as both solutes fully dissolve into DMSO.

3.2 Solar cell fabrication

Next, the steps for solar cell fabrication are presented. The cells are prepared according to Saliba et al. [24] The surface passivation method follows the protocol from the article “Anion optimization for bifunctional surface passivation in perovskite solar cells” by Xu et al. (2023). The idea of including bulk passivation in this work origins from the protocol from the article “Synergistic Crystallization and Passivation by a Single Molecular Additive for High-Performance Perovskite Solar Cells” by Du et al. (2022). The workflow for fabrication is presented in Figure 17.

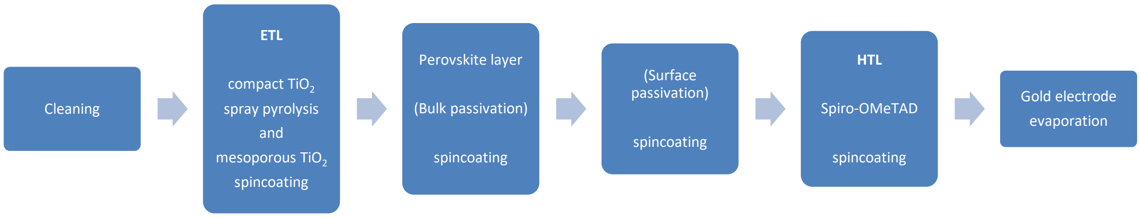

Figure 17. *Workflow for perovskite solar cell fabrication and their respective methods. Possible passivation steps shown in parenthesis.*

For the work, 2.2 mm thick TEC 15 FTO glass substrates from Greatcell Solar are used. The FTO substrates are first cleaned with 2% Mucasol solution while using a brush. After brushing, the substrates are then rinsed with tap water and with milli-Q water. Then, the substrates are put into an ultrasonic bath for 15 minutes in 30 °C in 2% Mucasol. The bath step is then redone with milli-Q water, acetone and isopropyl alcohol, respectively. In the last step, the substrates are dried under a nitrogen flow one by one and finally transferred into a clean Petri dish.

For the electron transport layer, first the compact TiO2 is deposited and after that a mesoporous TiO2. Before the deposition, the substrates are treated with UV-ozone for 15 minutes. The compact TiO2 solution is prepared by adding 6.5 ml of isopropyl alcohol to 1.5 ml of titanium di-isopropoxide bis(acetylacetonate) solution. When the UV-ozone treatment is completed, the substates can be transferred into the oven. Then, the substrates are heated to 450 °C. The solution for compact-TiO2 layer is deposited on the FTO substrates via spray pyrolysis. After the deposition the substrates are annealed at 450 °C for 45 minutes.

The mesoporous TiO2 solution is prepared one day before the deposition. For the solution, 300 mg of Greatcell Solar 30 NR-D titania paste and 2 ml undenatured ethanol are used. The solution is then left to stir overnight at room temperature. Next day, the substrates with compact TiO2 are collected and the mesoporous TiO2 solution is spin coated with speed of 4000 rpm for 10 seconds with acceleration of 2000 rpm/s by pipetting 80 µl on the centre of the substrate. Then, the substrate is moved on to a 100 °C hotplate for a few minutes before sintering. This is repeated for every substrate. For sintering, a program for the oven shown in Table 1 is used.

Table 1. *Sintering program for mesoporous TiO_2 layer.*

Ramp (min)	5	15	5	5	5
Temp (°C)	125	325	375	450	150
Hold (min)	5	5	5	30	∞

When the substrates are cooled down to ~200 °C in the last step of the sintering program, they are immediately taken out of the oven to a glass Petri dish and transferred into a N_2 filled glovebox for perovskite layer deposition. Both passivation techniques are presented in Figure 18 and Figure 19 .

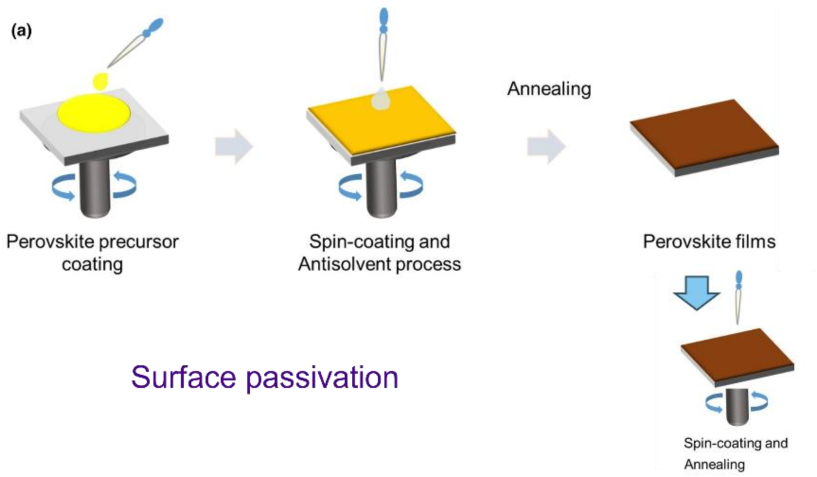

Figure 18. *Surface passivation workflow. Adapted from [31].*

The perovskite precursor solution is spin coated by spreading 60 µl to the substrate before starting then spinning at 1000 rpm for 10 seconds, followed by an acceleration at 6000 rpm for 20 seconds. While the program is running, 100 µl of anti-solvent chlorobenzene (CB) is pipetted on the substrate 5 seconds before the end of the program. After the spinning ends, the substrate is transferred on to the hotplate (100 °C) for 1 hour for the annealing step. After annealing and allowing the substrates to cool down to RT, the passivating layer can be applied to the surface of the perovskite by spin coating 130 µl of the passivating solution onto a substrate spinning at 4000 rpm. The spinning program lasts 25 seconds. After coating, the substrate is annealed at 105 °C for 5 minutes to remove the remaining IPA from the passivating layer. Then, the substrates are removed from the hotplate and kept inside the glovebox for the hole transfer layer deposition.

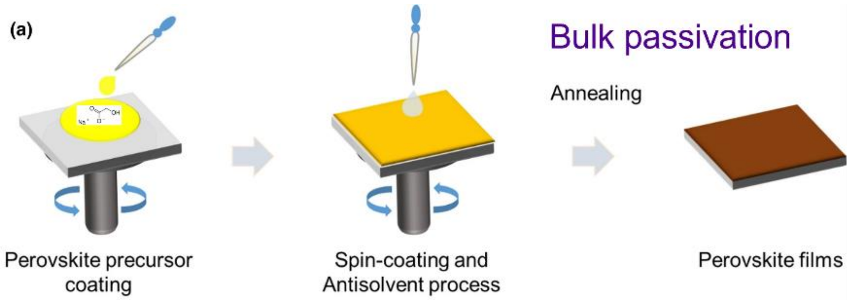

Figure 19. *Bulk passivation workflow. Adapted from [31].*

For the bulk passivation step shown in Figure 19, the passivation solution (0.5 mg/ml in DMSO) is added into the perovskite precursor in a 1 to 4% v/v (volume per volume) ratio, e.g., 5.4 µl of passivation solution to a 264.6 µl perovskite precursor to prepare a solution of 2% SHA or STG v/v in perovskite. The perovskite deposition is performed by spreading 60 µl on the substrate before starting the program, then spinning the substrate at 1000 rpm for 10 seconds, followed by an acceleration at 6000 rpm for 20 seconds. While the program is spinning, 100 µl of anti-solvent CB is pipetted on the substrate at 6000 rpm for 5 seconds before the end of the program. Then, the substrate is transferred into a 100 °C hotplate for 1 hour. After the annealing, the substrates are removed from the hotplate and kept inside the glovebox for HTL deposition.

The hole transport material used in this work is commercial Spiro-OMeTAD. For a batch, 36.15 mg of Spiro-OMeTAD is scaled and dissolved into 1 ml of chlorobenzene by heating the solution at 60 °C for a few minutes. After allowing the solution to cool down to room temperature, the dopants tBP (4-tertbutylpyridine), Li-TFSI (Lithium bis(trifluoromethanesulfonyl)imide), and FK209 (tris(2-(1*H*-pyrazol-1-yl)-4-*tert*-butylpyridine) cobalt (III) tri[bis(trifluoromethane)sulfonimide]) are added into the solution according to the specifications in Table 2. The dopant solutions are prepared by scaling Li-TFSI and FK209 and dissolving them into acetonitrile, targeting concentrations of 520 mg/ml for Li-TFSI and 300 mg/ml for FK209.

***Table 2.** Dopants and their amounts for Spiro-OMeTAD.*

Dopant	Amount (µl)
TBP	14.39
Li-TFSI	8.75
FK209	14.50

On top of the perovskite layer, or surface-passivated layer, 80 µl of Spiro-OMeTAD solution is spread at 1800 rpm for 30 seconds while spinning the substrate. After the program ends, the substrate is placed into a sample holder. When the deposition on all the substrates is complete, the samples are removed from the glovebox and placed into a dry box (<15-20 % relative humidity) overnight for the Spiro-OMeTAD oxidization.

For the solar cell device completion, a circuit needs to be formed between FTO and gold electrodes. For the last step, substrates are transferred into a masked holder for the gold electrode evaporation. The evaporation step is carried out by using MB-OPTIvap. Vacuum deposition is a beneficial way to control the thickness of the gold layer and ensure uniform and pinhole-free films. The gold is evaporated at a controlled rate with a target of an approximately 100 nm thick on the top of the other previously deposited device layers. The devices are then removed from the chamber and transferred to a dry box for overnight.

3.3 Solar cell performance and characterization

The performance and the characteristics of perovskite solar cells can be studied with a wide variety of different techniques. To evaluate the performance of the solar cells, J-V measurements are carried out to obtain the PV parameters known as PCE, FF, J_{SC} and V_{OC}. The reliability of PV parameters can be examined by measuring the external quantum efficiency (EQE) of the cells. The mismatch between the short circuit currents should be less than 20% under 1-Sun illumination for the results to be thought as reliable. [37] The maximum power point tracking characterization can be used to study the devices stress resistance to continuous illumination and understand how the PV parameters change as a function of time.

To determine the perovskite band gap, absorption spectra are recorded using a UV-Vis spectrophotometer. Imaging the surface of the perovskite layer with a scanning electron microscope (SEM) helps assess possible changes in the crystal size of the perovskite films resulting from the passivation methods. To study the crystal structure even further, X-ray diffraction is a very useful tool for evaluating whether passivation causes changes to the crystal structure or crystallinity of the samples.

The Litos Lite system (FLUXiM AG, Switzerland) is used to record the reverse and forward J-V sweeps with a scan rate of 50 mV/s. Also, the maximum power point tracking is performed under simulated sunlight. An A++A+A solar simulator (Sinus LED simulator from Wavelabs) is used to generate the AM 1.5G simulated sunlight. The J-V scans and stable power output (SPO) were measured in ambient air and MPPT is performed under nitrogen (N_2) atmosphere. Aperture masks for the devices have an area of 7mm^2.

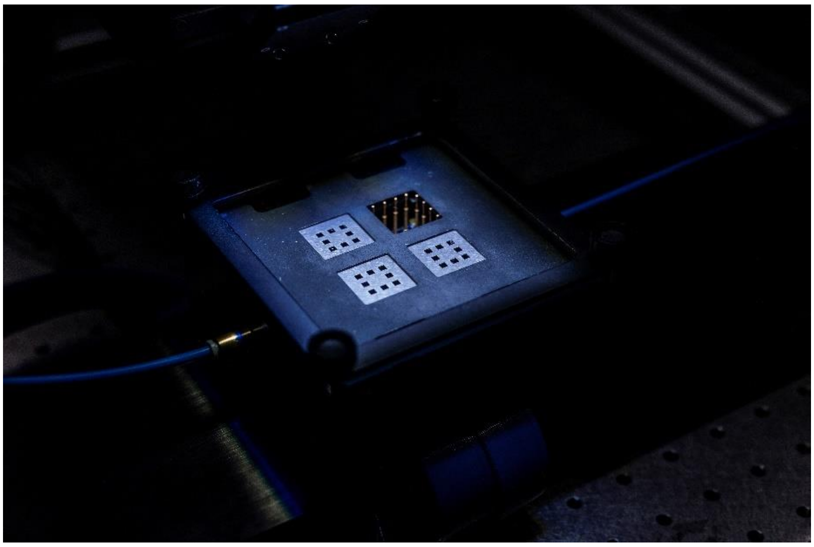

Figure 20. *Sample holder for Litos Lite solar simulator.*

Before measurements, the samples are first placed inside a dry box and then exposed to ambient air. The 7mm^2 mask is inserted on top of cells before illumination. The mask is shown in Figure 20. After the masks are aligned, the sample holder can be placed under illumination. The measurement scans go from reverse to forward direction, from -0.2 to 1.2 V, at a scan rate of 50 mV/s. After the measurement, all the results (*PCE*, *FF*, J_{SC} and V_{OC}) are readily displayed on the screen and are further extracted into a memory stick for the analysis. From the results, the best (device) pixels are selected for EQE characterization to verify the reliability of the measurements. For indoor measurements, a custom-made setup shown in Figure 21 is used.

Figure 21. *Indoor measurement setup of the HSC group.*

In the bottom part of Figure 21, a sample holder for the device is shown. One pixel from each sample is measured at the time. The device is covered with a 7 mm^2 mask and aligned to avoid any light scattering that affects the measurement. A Phillips HUE WLED bulb with adjustable color temperature and light intensity was used for indoor measurements at 4000 K temperature. The bulb can be controlled with a mobile application. The intensity of the light is measured with a digital light intensity meter before the indoor measurements. The measurement is controlled by a MATLAB script and a Keithley SMU SourceMeter. The measurement range is from 1.2 V to -0.2 V with forward and backward scans. For measuring short maximum power point tracking, the script is slightly modified.

Light intensity dependence characterization is performed by changing the light intensity of the lamp by using the external mobile application. The true intensity of the light is accurately determined with a BiTec Sensor Luxmeter before every measurement. All the data from the indoor measurements can be again accessed with the results compiler app within MATLAB.

The absorbance of perovskite films can be measured with a UV-Vis spectrophotometer Shimadzu UV-1900i. For the measurement, samples are prepared on glass substrates. Glass substrates are first cleaned with the same procedure as for the FTO substrates. Before transferring the glass substrates into a N_2 filled glovebox, the substrates need to be cleaned with UV-ozone for 15 minutes. Then, the substrates are spin coated with the same settings as the perovskite layer on FTO (for device fabrication). After spin coating, the glass substrates are transferred onto a 100 °C hotplate for 1 hour. Then, depending on whether the sample is surface or bulk passivated, it is either placed into a Petri dish to wait for measurement or surface passivated in the same manner as it would be on the device.

For measurement, the samples are placed into the sample holder of the machine and measured between the wavelengths of 300 nm and 900 nm. The data is then saved on a memory stick and analysed later.

To confirm the reliability of the J-V-measurements, EQE must be measured. EQE is the ratio of the number of charge carriers to the amount of incident photons. The measurement is performed using the Newport Quantx-300 Quantum efficiency measurement system. For the measurement, a few of the best-performing pixels are selected and measured individually. From the measurement, an EQE curve is obtained, and the short-circuit current from the EQE measurement ($J_{SC,\ EQE}$) is compared to the $J_{SC,\ J\text{-}V}$ from the J-V-measurement. If the mismatch between the results is under 20%, the results are considered reliable.

The crystallinity of perovskite is of utmost importance, as an imperfect crystal structure is prone to defects. When using bulk passivation, the crystalline structure of perovskite could be altered, potentially affecting its ability to generate electrons and holes. The system used is the Panalytical Empyrean Multipurpose Diffractometer. For XRD analysis, the samples are prepared on FTO with the perovskite layer on top. The sample is bombarded with X-rays, and the angles at which the X-rays are diffracted are measured. The results can be compared between the reference and the bulk-passivated devices to determine if the passivation alters the crystallinity.

4. RESULTS

In this chapter, the key results of the thesis are presented. In the first section, the determination of the best concentration for surface passivation agents is presented and in the next section similar optimization is discussed for bulk passivation. To find out the best passivation method, the PV performance under different concentrations of the passivating molecules is studied. In the last section, the passivated perovskite solar cells are characterized by measuring external quantum efficiency, absorption spectra, X-ray diffraction, scanning electron microscopy. The stress resistance test for bulk passivated devices is done under 1-Sun and lastly, the effect of passivation is studied under low light intensities.

4.1 Surface passivation

In this section, the performance of devices from different solar cell batches is reported, with a focus on the effect of surface passivation upon the introduction of sodium thioglycolate and sodium hydroxyacetate. The best 20 devices are presented for each case. The photovoltaic parameters extracted from the recorded J-V-characteristics under 1-Sun and indoor (white LED) illumination are reported. Results for sodium thioglycolate (STG) surface passivator are presented in Figure 22 and in Table 3.

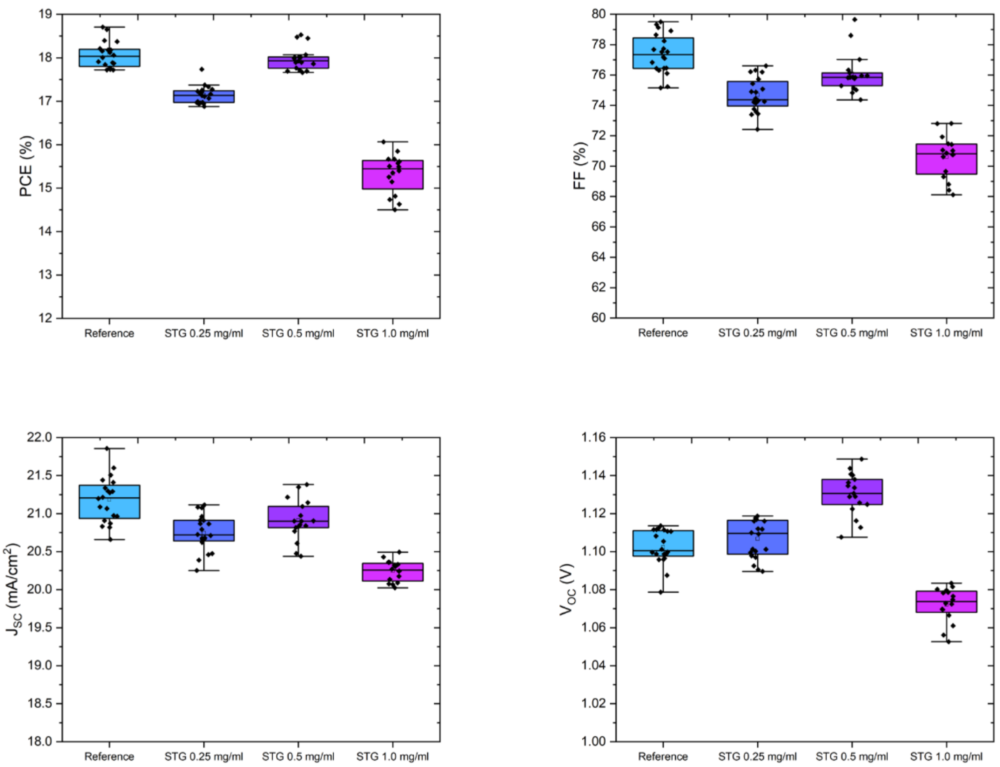

Figure 22. *Top 20 devices including sodium thioglycolate (STG) surface passivating molecule under 1-Sun illumination.*

Table 3. *Average photovoltaic parameters for STG top 20 surface passivated devices under 1-Sun illumination. Best pixels are shown in brackets.*

Type	PCE (%)	FF (%)	J_{sc} (mA/cm^2)	V_{oc} (V)	HI (%)
Reference	18.06 ± 0.3 (18.71)	77.37 ± 1.3 (79.32)	21.18 ± 0.3 (21.21)	1.10 ± 0.01 (1.11)	14.77 ± 5.3 (9.33)
STG 0.25 mg/ml	17.14 ± 0.2 (17.74)	74.68 ± 1.1 (76.32)	20.74 ± 0.2 (20.79)	1.11 ± 0.01 (1.12)	14.08 ± 3.8 (12.15)
STG 0.50 mg/ml	17.86 ± 0.4 (18.53)	75.81 ± 1.4 (79.65)	20.91 ± 0.2 (20.44)	1.13 ± 0.01 (1.14)	15.37 ± 4.2 (23.08)
STG 1.0 mg/ml	15.22 ± 0.5 (16.06)	70.83 ± 1.3 (72.80)	20.03 ± 1.3 (20.43)	1.07 ± 0.01 (1.08)	15.63 ± 1.9 (14.27)

From the results, an increase in V_{OC} can be observed when using 0.5 mg/ml of the passivating molecule compared to the reference device. Surface passivated samples with 0.5 mg/ml of STG are the most promising. For surface passivation with sodium hydroxyacetate, the results are shown in Figure 23 and Table 4.

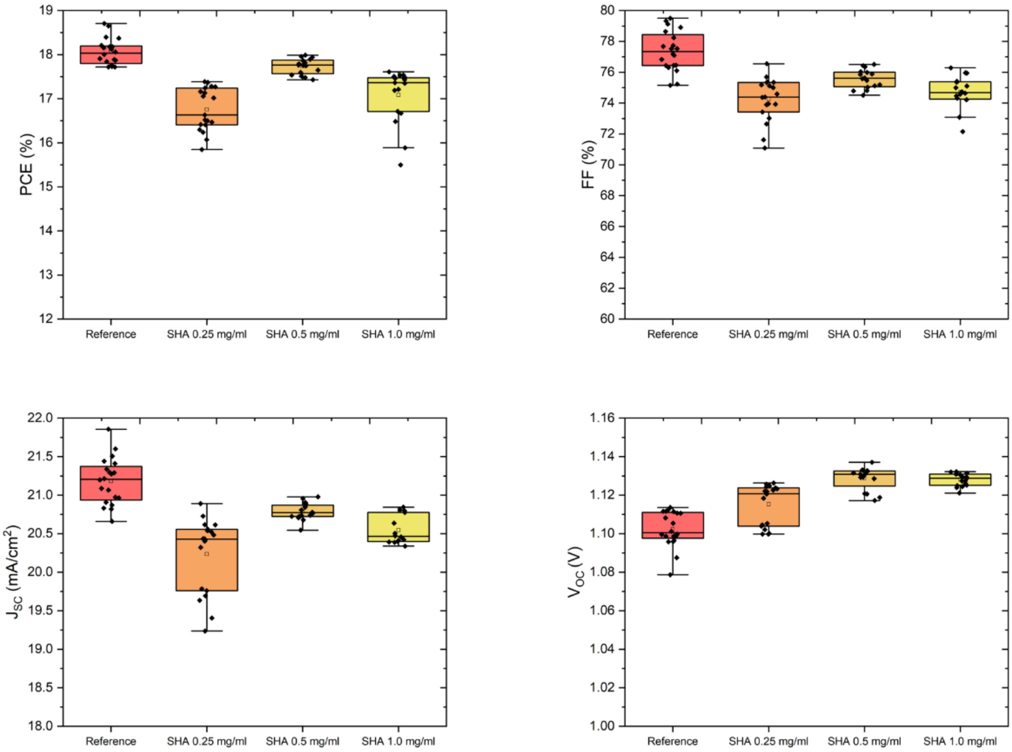

Figure 23. *Top 20 devices including sodium hydroxyacetate (SHA) surface passivating molecule under 1-Sun illumination.*

Table 4. *Average photovoltaic parameters for SHA top 20 surface passivated devices under 1-Sun illumination. Best pixels are shown in brackets.*

Type	PCE (%)	FF (%)	J_{sc} (mA/cm^2)	V_{oc} (V)	HI (%)
Reference	18.06 ± 0.3 (18.71)	77.37 ± 1.3 (79.32)	21.18 ± 0.3 (21.21)	1.10 ± 0.01 (1.11)	14.77 ± 5.3 (9.33)
SHA 0.25 mg/ml	16.69 ± 0.5 (17.39)	73.92 ± 1.9 (75.69)	20.25 ± 0.5 (20.40)	1.11 ± 0.01 (1.13)	12.37 ± 3.0 (16.83)
SHA 0.50 mg/ml	17.70 ± 0.2 (17.99)	75.28 ± 0.8 (75.99)	20.99 ± 0.4 (20.91)	1.12 ± 0.02 (1.13)	10.02 ± 2.2 (9.19)
SHA 1.0 mg/ml	16.86 ± 0.8 (17.61)	73.80 ± 0.8 (76.23)	20.28 ± 0.5 (20.39)	1.13 ± 0.01 (1.13)	9.83 ± 1.7 (9.20)

Here the 0.5 mg/ml condition proves to slightly improve V_{OC}. Again, compared to the other conditions the 0.5 mg/ml is the most promising concentration.

Both STG and SHA behaved similarly under the 1-Sun measurement. Xu et al. also experienced the biggest increase in V_{OC} in their study, which is interesting as their passivation is done in an inverted structure between perovskite and ETL unlike in this study where the passivation is between the perovskite and HTL. This is suggesting an idea that the passivation could also be studied in a sandwich-like structure, where the perovskite is surface passivated from both sides. [32]

The effect of surface passivation is also evaluated in devices under indoor lighting at 1000 lux, 4000 K. Results for the top 20 devices including sodium thioglycolate passivator are presented in Figure 24 and Table 5.

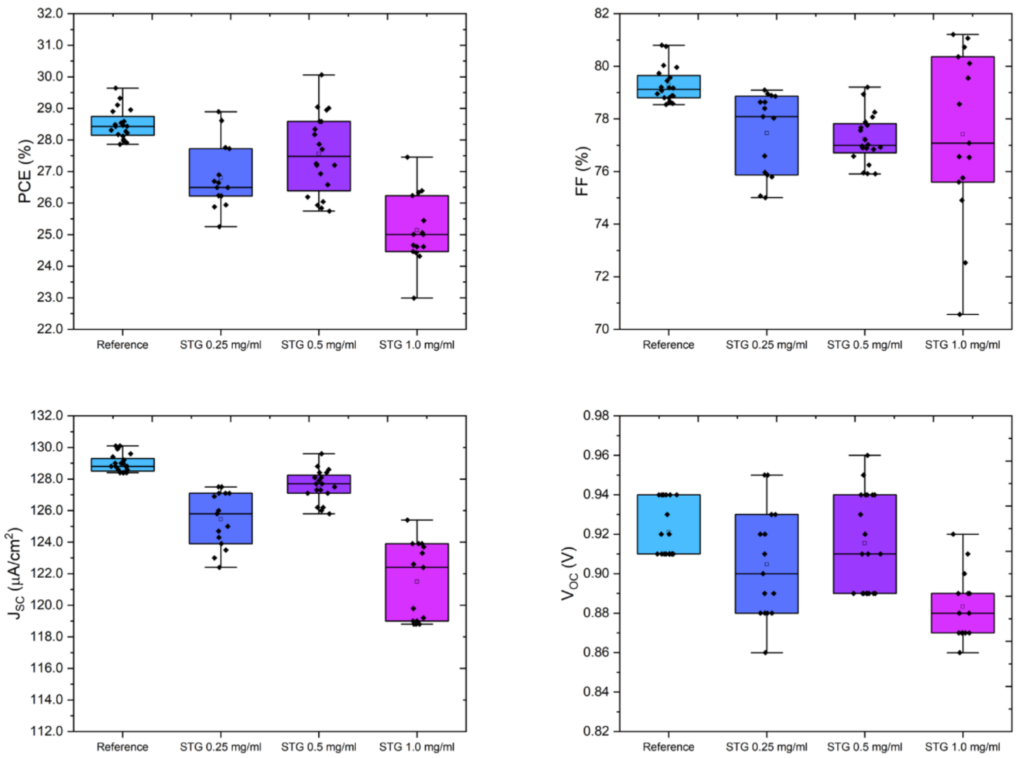

Figure 24. *Top 20 devices including sodium thioglycolate (STG) surface passivating molecule under indoor illumination at 1000 lux.*

Table 5. *Average photovoltaic parameters for top 20 sodium thioglycolate surface passivated devices under indoor lighting at 1000 lux. Best pixels are shown in brackets.*

Type	PCE (%)	FF (%)	J_{sc} (μA/cm²)	V_{oc} (V)	HI (%)
Reference	28.49 ± 0.5 (29.64)	77.66 ± 1.2 (78.87)	128.25 ± 1.0 (127.90)	0.92 ± 0.02 (0.94)	12.04 ± 5.5 (4.84)
STG 0.25 mg/ml	26.43 ± 1.2 (28.90)	76.13 ± 3.4 (76.60)	124.24 ± 2.3 (127.10)	0.90 ± 0.03 (0.95)	9.92 ± 4.8 (7.44)
STG 0.50 mg/ml	27.56 ± 1.2 (30.06)	76.50 ± 2.1 (78.07)	126.42 ± 1.9 (128.40)	0.91 ± 0.03 (0.96)	14.60 ± 7.2 (15.21)
STG 1.0 mg/ml	24.36 ± 1.6 (27.45)	75.33 ± 4.5 (77.08)	119.53 ± 2.8 (123.90)	0.87 ± 0.03 (0.92)	16.04 ± 7.2 (21.77)

Results have quite a bit of variation. Here, the passivation with a concentration of 0.5 mg/ml has the best pixel with *PCE* being over 30%. There are no noticeable improvements on average with the surface passivation under indoor illumination with sodium thioglycolate. Results for surface passivation with sodium hydroxyacetate are presented in Figure 25 and Table 6.

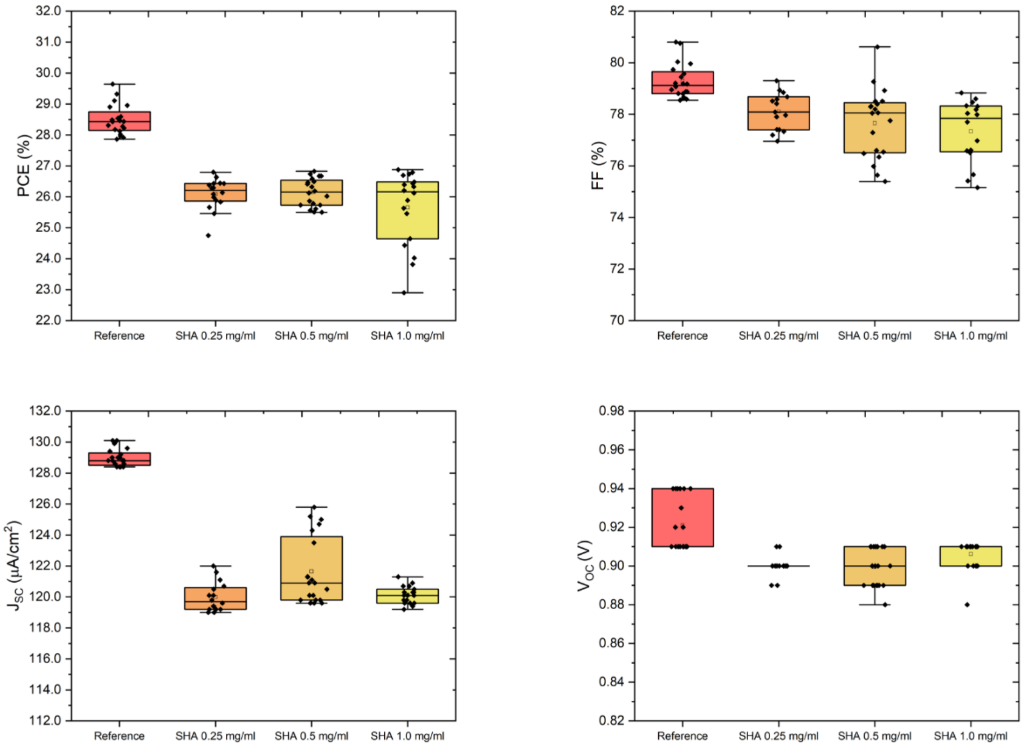

Figure 25. *Top 20 devices including sodium hydroxyacetate (SHA) surface passivating molecule under indoor illumination at 1000 lux.*

Table 6. *Average photovoltaic parameters for top 20 sodium hydroxyacetate surface passivated devices under indoor lighting at 1000 lux. Best pixels are shown in brackets.*

Type	PCE (%)	FF (%)	J_{sc} (µA/cm²)	V_{oc} (V)	HI (%)
Reference	28.49 ± 0.5 (29.64)	77.66 ± 1.2 (78.87)	128.25 ± 1.0 (127.90)	0.92 ± 0.02 (0.94)	12.04 ± 5.5 (4.84)
SHA 0.25 mg/ml	25.87 ± 1.0 (26.80)	77.13 ± 2.9 (78.93)	119.34 ± 0.7 (120.70)	0.90 ± 0.01 (0.90)	12.97 ± 3.8 (16.80)
SHA 0.50 mg/ml	26.14 ± 0.4 (26.83)	77.56 ± 1.5 (78.29)	120.97 ± 2.3 (120.50)	0.89 ± 0.02 (0.91)	11.14 ± 3.3 (11.90)
SHA 1.0 mg/ml	25.14 ± 1.9 (26.88)	75.14 ± 4.9 (78.31)	118.61 ± 3.4 (120.70)	0.90 ± 0.01 (0.91)	10.72 ± 3.4 (12.00)

Comparing the SHA surface passivation to the reference, there are no noticeable improvements within any of the parameters.

Comparing surface passivation under 1-Sun against indoor illumination an overall increase in fill factor can be noticed. This is probably due to the higher shunt resistance which is important for the photovoltaic performance under indoor illumination. [13]

4.2 Bulk passivation

In this section, results for different batches of bulk with both molecules are combined and top 20 pixels of every condition are presented. Photovoltaic parameters under 1-Sun and indoor illumination are both covered. Starting with surface passivation with sodium thioglycolate. The results for measurements under 1-Sun are presented in Figure 26 and in Table 7.

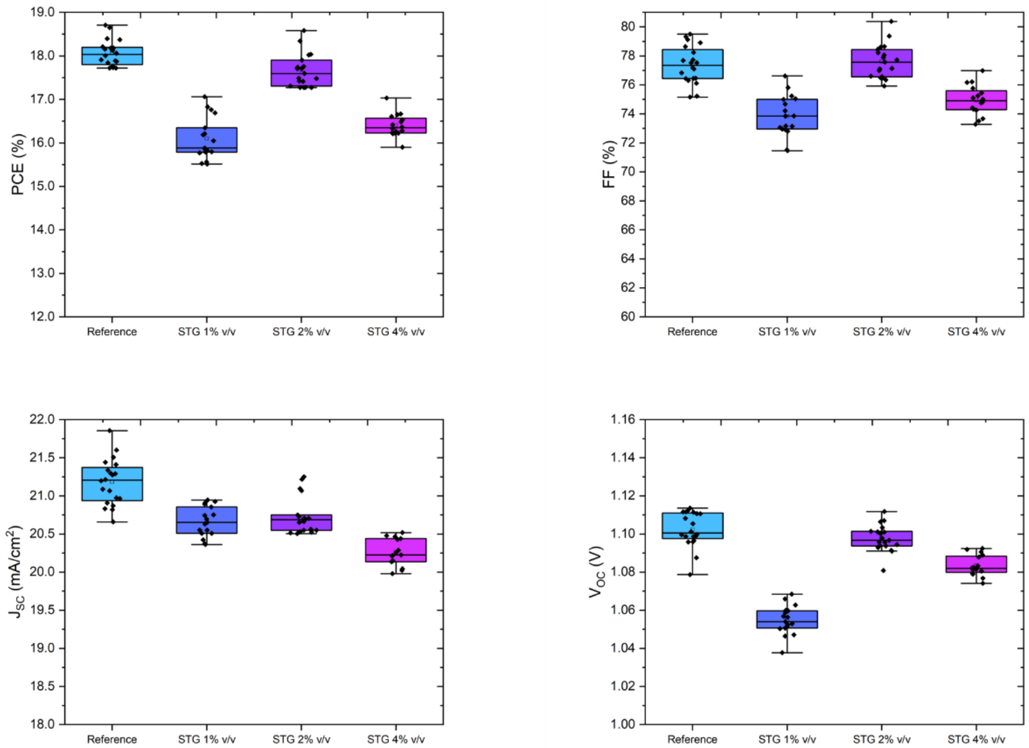

Figure 26. *Top 20 devices including sodium thioglycolate (STG) bulk passivating molecule under 1-Sun. Abbreviation v/v stands for volume per volume.*

Table 7. *Average photovoltaic parameters for top 20 sodium thioglycolate bulk passivated devices under 1-Sun. Best pixels are shown in brackets.*

Type	PCE (%)	FF (%)	J_{sc} (mA/cm^2)	V_{oc} (V)	HI (%)
Reference	18.06 ± 0.3 (18.71)	77.37 ± 1.3 (79.32)	21.18 ± 0.3 (21.21)	1.10 ± 0.01 (1.11)	14.77 ± 5.3 (9.33)
STG 1% v/v	16.07 ± 0.5 (17.06)	74.16 ± 1.5 (76.61)	20.51 ± 0.4 (20.89)	1.06 ± 0.01 (1.07)	9.80 ± 2.3 (12.18)
STG 2% v/v	17.65 ± 0.4 (18.58)	77.64 ± 1.1 (78.64)	20.70 ± 0.3 (21.25)	1.10 ± 0.01 (1.11)	12.45 ± 5.4 (10.40)
STG 4% v/v	16.12 ± 0.6 (17.03)	74.80 ± 1.0 (76.17)	19.91 ± 0.7 (20.48)	1.08 ± 0.01 (1.09)	17.72 ± 0.5 (17.29)

Bulk passivation slightly improves the *FF* on average with 2% v/v condition. The 2% v/v condition is better compared to two other conditions. Seeing a minor improvement in fill factor could mean that the passivation slightly improves the charge transport and extraction efficiency. [1] For bulk passivation with sodium hydroxyacetate (SHA) the results are shown in Figure 27 and in Table 8.

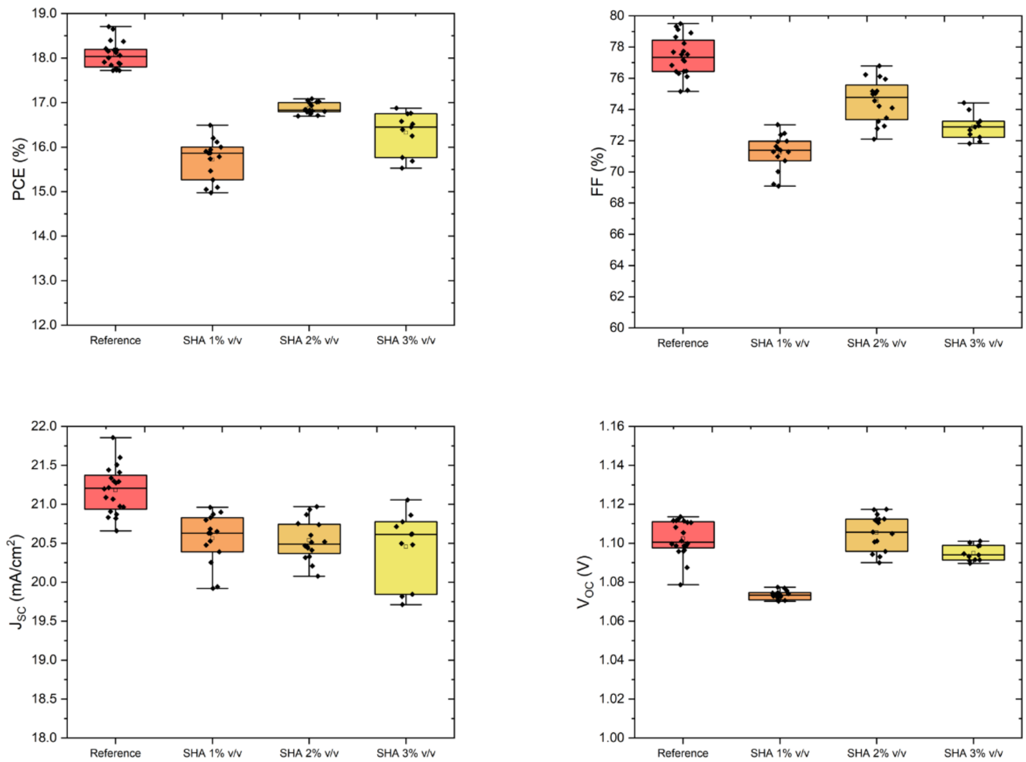

Figure 27. *Top 20 devices including sodium hydroxyacetate (SHA) bulk passivating molecule under 1-Sun. Abbreviation v/v stands for volume per volume.*

Table 8. *Average photovoltaic parameters for top 20 sodium hydroxyacetate bulk passivated devices under 1-Sun. Best pixels are shown in brackets.*

Type	PCE (%)	FF (%)	J_{sc} (mA/cm²)	V_{oc} (V)	HI (%)
Reference	18.06 ± 0.3 (18.71)	77.37 ± 1.3 (79.32)	21.18 ± 0.3 (21.21)	1.10 ± 0.01 (1.11)	14.77 ± 5.3 (9.33)
SHA 1% v/v	15.37 ± 0.8 (16.49)	70.27 ± 2.8 (73.02)	20.43 ± 0.5 (20.96)	1.07 ± 0.01 (1.08)	19.86 ± 2.1 (21.32)
SHA 2% v/v	16.83 ± 0.1 (17.08)	74.56 ± 1.2 (76.79)	20.56 ± 0.2 (20.41)	1.10 ± 0.02 (1.09)	16.61 ± 5.5 (22.48)
SHA 3% v/v	15.94 ± 1.1 (16.87)	71.59 ± 3.1 (74.43)	20.49 ± 0.4 (20.71)	1.09 ± 0.03 (1.09)	16.42 ± 6.0 (16.58)

Under 1-Sun sodium hydroxyacetate does not improve the photovoltaic parameters with any conditions. Below the indoor results for both molecules are presented. The results for sodium thioglycolate are shown in Figure 28 and in Table 9.

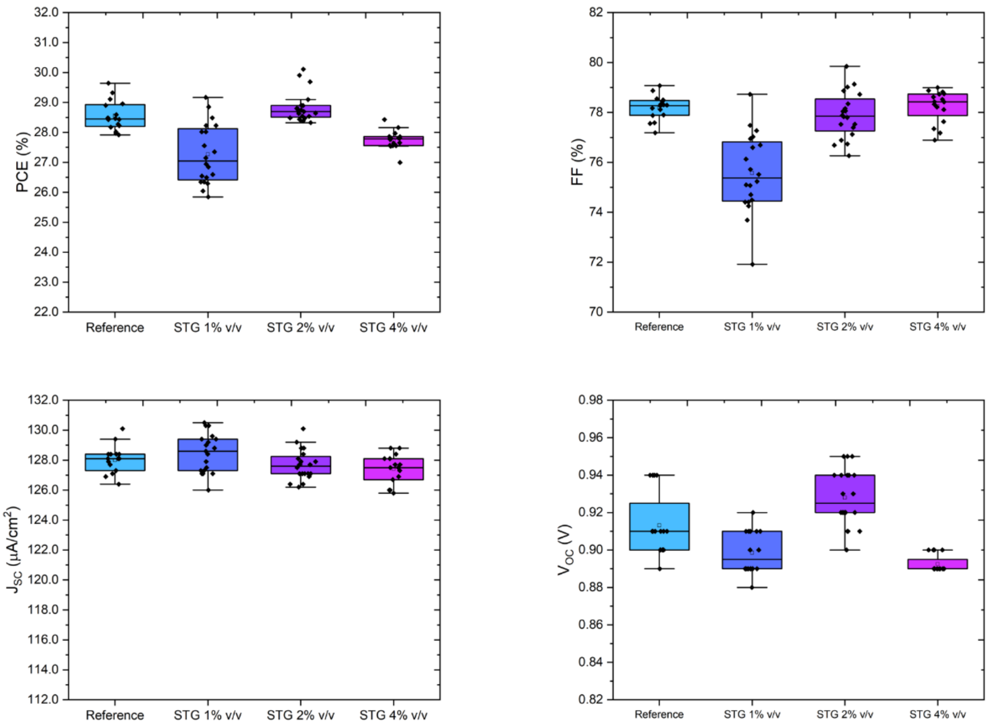

Figure 28. *Top 20 devices including sodium thioglycolate (STG) bulk passivating molecule under indoor illumination at 1000 lux. Abbreviation v/v stands for volume per volume.*

Table 9. *Average photovoltaic parameters for top 20 pixels sodium thioglycolate bulk passivated under indoor illumination at 1000 lux. Best pixels are shown in brackets.*

Type	PCE (%)	FF (%)	J_{sc} (μA/cm^2)	V_{oc} (V)	HI (%)
Reference	28.49 ± 0.5 (29.64)	77.66 ± 1.2 (78.87)	128.25 ± 1.0 (127.90)	0.92 ± 0.02 (0.94)	12.04 ± 5.5 (4.84)
STG 1% v/v	27.27 ± 1.0 (29.17)	75.57 ± 1.5 (78.73)	128.47 ± 1.2 (130.30)	0.90 ± 0.01 (0.91)	22.69 ± 6.0 (26.55)
STG 2% v/v	28.84 ± 0.5 (30.11)	77.89 ± 0.9 (79.02)	127.68 ± 1.0 (128.40)	0.93 ± 0.01 (0.95)	12.15 ± 6.7 (7.30)
STG 4% v/v	27.47 ± 0.6 (28.43)	78.15 ± 0.6 (78.88)	126.11 ± 1.5 (128.10)	0.89 ± 0.004 (0.90)	15.14 ± 2.6 (19.43)

Based on the indoor measurements the best indoor pixel is 2% v/v bulk passivated with STG having slight improvements in *PCE*, *FF* and V_{OC}. Also, the condition with 1% v/v proves to improve the J_{SC}, but unfortunately the performance is decreased with other parameters. The base of the improvement with sodium thioglycolate is the increase in *FF*, which could be explained by the reduction in trap-assisted recombination rate. [33]

Below the results for indoor measurements for sodium hydroxyacetate are presented in Figure 29 and Table 10.

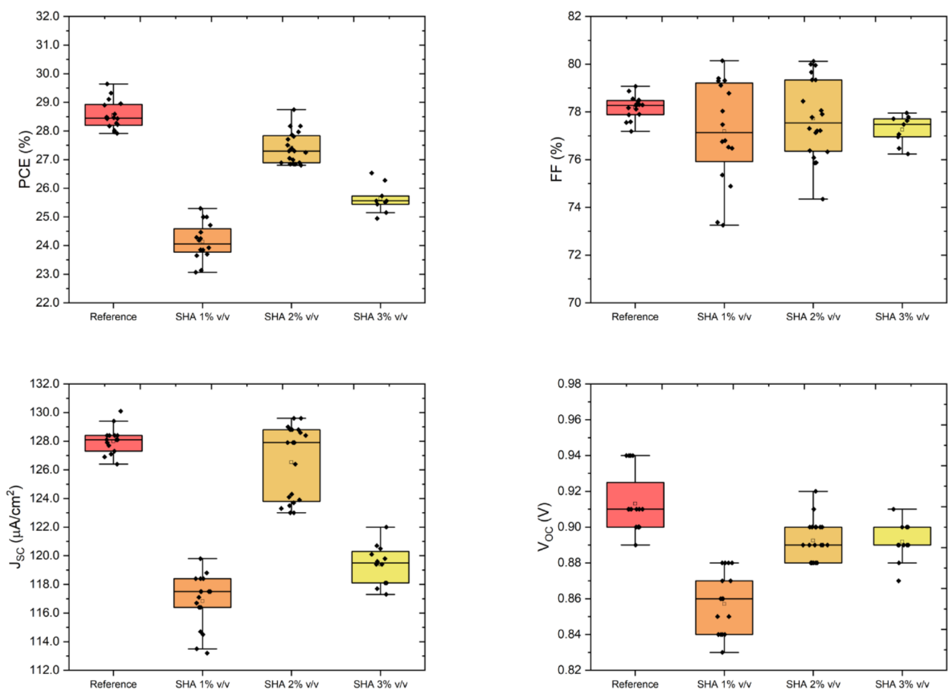

Figure 29. *Top 20 devices including sodium hydroxyacetate (SHA) bulk passivating molecule under indoor illumination at 1000 lux. Abbreviation v/v stands for volume per volume.*

Table 10. *Average photovoltaic parameters for top 20 sodium hydroxyacetate bulk passivated under indoor lighting at 1000 lux. Best pixels are shown in brackets.*

Type	PCE (%)	FF (%)	J_{sc} (μA/cm^2)	V_{oc} (V)	HI (%)
Reference	28.49 ± 0.5 (29.64)	77.66 ± 1.2 (78.87)	128.25 ± 1.0 (127.90)	0.92 ± 0.02 (0.94)	12.04 ± 5.5 (4.84)
SHA 1% v/v	23.98 ± 0.9 (25.30)	76.67 ± 2.9 (76.75)	116.84 ± 1.8 (119.80)	0.86 ± 0.02 (0.88)	12.70 ± 4.7 (16.02)
SHA 2% v/v	27.42 ± 0.5 (28.75)	77.72 ± 1.6 (77.13)	126.53 ± 2.5 (129.60)	0.89 ± 0.01 (0.92)	21.74 ± 3.4 (21.97)
SHA 3% v/v	24.58 ± 1.9 (24.58)	74.30 ± 5.5 (77.71)	119.39 ± 1.3 (120.10)	0.89 ± 0.02 (0.91)	12.57 ± 7.7 (16.87)

Under indoor illumination the condition 2% v/v is superior compared to other passivation conditions on average on every category. Also, a slight improvement in *FF* against the reference on average, which could state the decrease in trap-assisted recombination rate also with this passivation method. [33] To confirm the reliability of the measurements during the work period, external quantum efficiency was measured for a reference sample and for the best passivating concentration for both molecules in both techniques in their respective batches. Results for the measurements are shown in Figure 30 and Table 11.

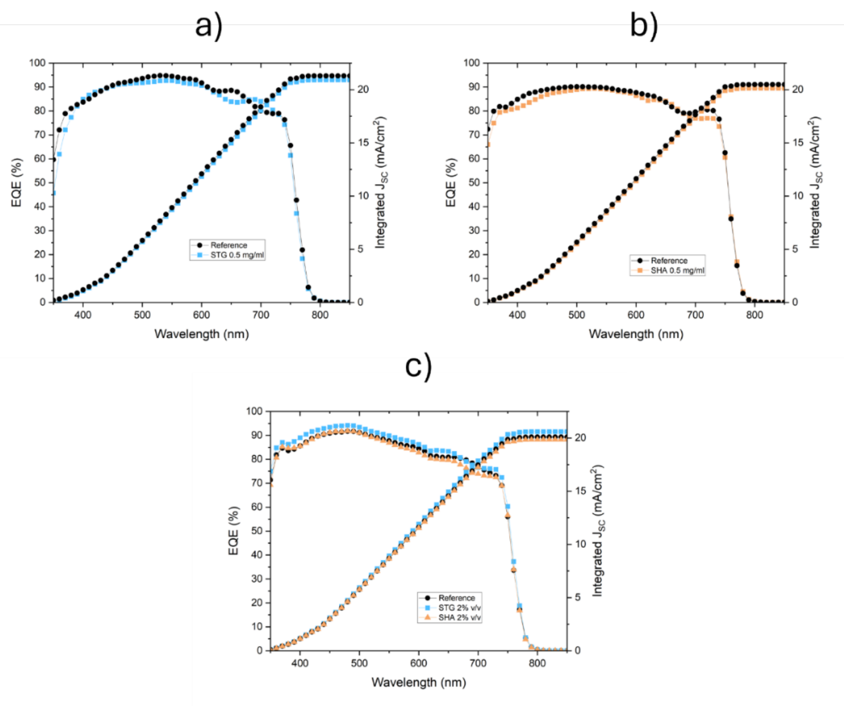

Figure 30. *Results for EQE measurements and the integrated J_{SC} curves for all conditions in their respective batches. a) Reference and surface passivated 0.5 mg/ml sodium thioglycolate b) Reference and surface passivated 0.5 mg/ml sodium hydroxyacetate and c) Reference and bulk passivated 2% v/v both molecules.*

Table 11. *Results for EQE measurements. a) Reference and surface passivated 0.5 mg/ml sodium thioglycolate b) Reference and surface passivated 0.5 mg/ml sodium hydroxyacetate and c) Reference and bulk passivated 2% v/v both molecules.*

a)

Type	$J_{sc,JV}$ (mA/cm²)	$J_{sc,EQE}$ (mA/cm²)	Mismatch (%)
Reference	21.07	21.53	2.2
STG 0.5 mg/ml	20.44	21.14	3.4

b)

Type	$J_{sc,JV}$ (mA/cm²)	$J_{sc,EQE}$ (mA/cm²)	Mismatch (%)
Reference	20.87	20.64	1.1
SHA 0.5 mg/ml	20.91	20.03	4.4

c)

Type	$J_{sc,JV}$ (mA/cm²)	$J_{sc,EQE}$ (mA/cm²)	Mismatch (%)
Reference	19.56	20.25	3.5
STG 2% v/v	21.00	20.76	1.2
SHA 2% v/v	20.12	20.01	0.5

The mismatch between the EQE and J-V-measurements is well under 20% for every condition, therefore the measurements can be considered reliable.

The best pixels J-V curves under 1-Sun with both passivation strategies and for both molecules are shown in Figure 31 and Table 12.

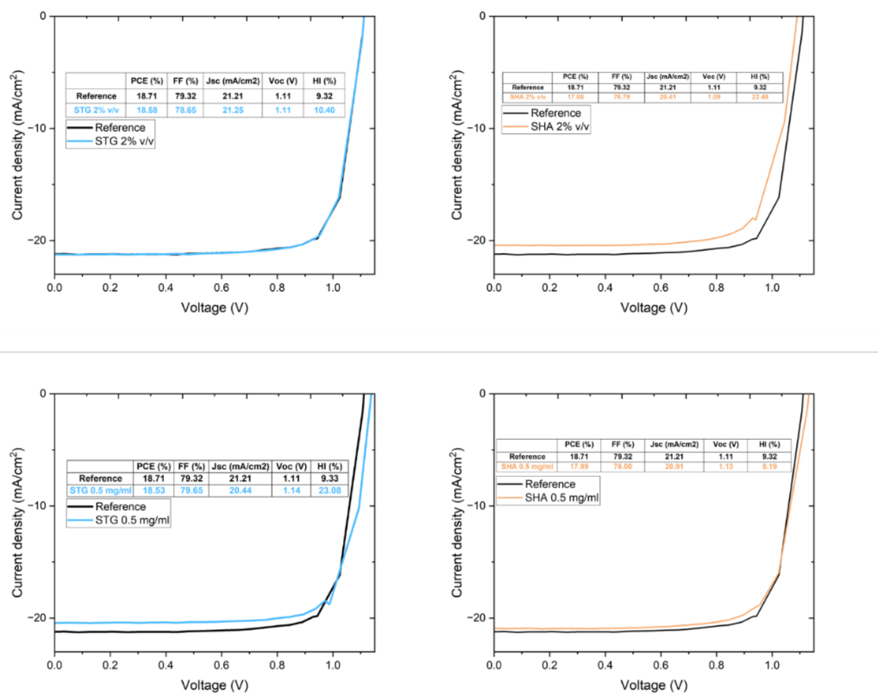

Figure 31. *J-V curves under 1-Sun for reference, STG, and SHA devices.*

Table 12. *Table of results for best individual pixel for measurements under 1-Sun.*

Type		PCE (%)	FF (%)	J_{SC} (mA/cm²)	V_{OC} (V)	HI (%)
Reference		18.71	79.32	21.21	1.11	9.32
Bulk passivation	STG 2% v/v	18.58	78.65	21.25	1.11	10.40
	SHA 2% v/v	17.08	76.79	20.41	1.09	22.48
Surface passivation	STG 0.5 mg/ml	18.53	79.65	20.44	1.14	23.08
	SHA 0.5 mg/ml	17.99	76.00	20.91	1.13	9.19

As can be seen from the results, sodium thioglycolate is more promising passivating molecule being far superior to sodium hydroxyacetate. For indoor measurements (1000 lux, 4000 K) the results are presented in Figure 32 and in Table 13.

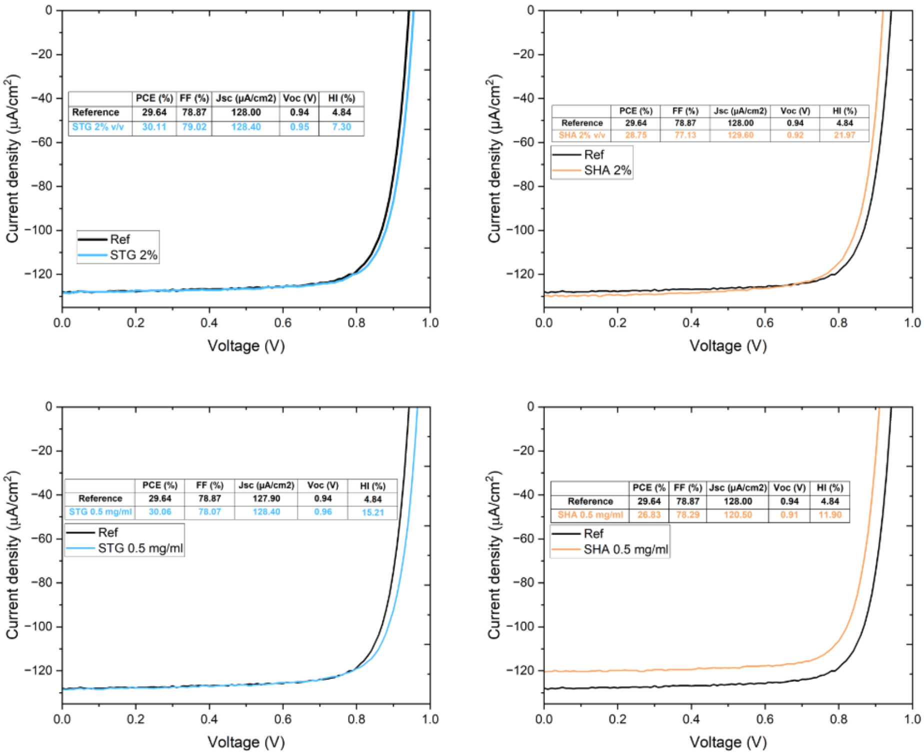

Figure 32. *J-V curves under indoor illumination at 1000 lux for reference, STG, and SHA devices.*

Table 13. *Table of results for best individual pixel for measurements under indoor illumination at 1000 lux.*

Type		PCE (%)	FF (%)	J_{SC} (μA/cm^2)	V_{OC} (V)	HI (%)
Reference		29.64	78.87	128.00	0.94	4.84
Bulk passivation	STG 2% v/v	30.11	79.02	128.40	0.95	7.30
	SHA 2% v/v	28.75	77.13	129.60	0.92	21.97
Surface passivation	STG 0.5 mg/ml	30.06	78.07	128.40	0.96	15.21
	SHA 0.5 mg/ml	26.83	78.29	120.50	0.91	11.90

Under indoor illumination the overall best performing pixels are from sodium thioglycolate STG in both passivation strategies. Bulk passivated sample with STG is slightly improved in every parameter. These results suggest the importance of investigating bulk passivation in devices at low light intensity illumination conditions to further understand the effects of passivation.

Comparing surface and bulk passivation strategies both have the potential to improve the performance of the solar cell. With surface passivation the V_{OC} increases under 1-Sun with both molecules and under indoor conditions with STG. Noticeable change against surface passivation is the bulk passivated samples increase in *FF*, which could be due to the small organic molecules fitting inside the perovskite and filling the donor-like defects and passivating the acceptor-like defects. [32] However, with both passivation strategies under 1-Sun illumination there are losses in short-circuit current J_{SC}, which directly affects the PCE-value of the cell. The losses with these passivation methods could be due to the high ionic loss, which could be due to high hysteresis. [29]

4.3 Characterization

In this section, results for absorption, X-ray diffraction (XRD), scanning electron microscopy (SEM) and maximum power point tracking (MPPT) are covered. For both molecules, the absorption spectra and scanning electron microscopy images are presented and analysed. For bulk passivation also the XRD analysis is performed.

Results for the absorbance measurements for both passivation strategies are presented for sodium thioglycolate (STG) and sodium hydroxyacetate (SHA) in Figure 33.

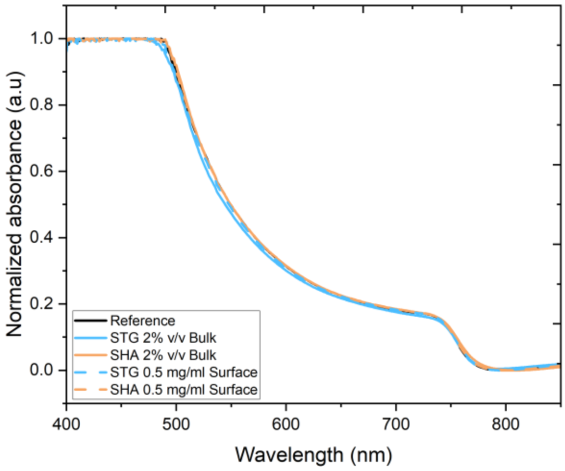

Figure 33. *Absorbance spectra for sodium thioglycolate and sodium hydroxyacetate for both passivation methods.*

From the absorption spectra in Figure 33, the band gaps for the perovskite are calculated and for every condition the band gap is 1.60 eV. [14] Therefore, passivation does not alter the perovskites band gap as the results are the same for each condition. In general perovskite solar cells have a band gap between 1.48 eV to 1.62 eV. [17] In literature, for the perovskite layer composition of $Cs_{0.05}(MA_{0.17}FA_{0.83})_{0.95}Pb(I_{0.83}Br_{0.17})_3$ a band gap of 1.62 eV has been reported. [25]

From the solar cell performance experiments, we can conclude that the bulk passivation method is more promising due to the better performance under indoor illumination, and because of the easier solubility of the compound in dimethyl sulfoxide (DMSO). Therefore, additional characterization was performed to study the effects of this passivation method. X-ray diffraction analysis was done to confirm that the perovskite crystal structure stays unchanged.

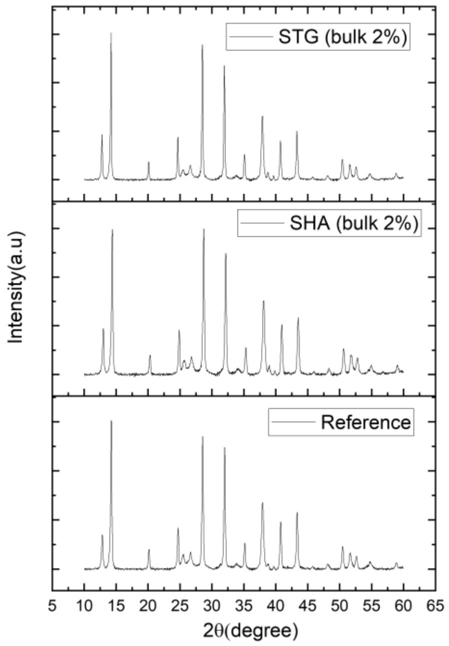

Figure 34. *XRD patterns of bulk passivated devices.*

In Figure 34, we can confirm that the crystal structure stays unchanged. Also, the X-site passivation in perovskite crystals with pseudohalides according to Xu et al. avoids the formation of lower-dimensional phases. From XRD analysis it can be confirmed that bulk passivation does not form these deleterious lower-dimensional phases. [32] Using small organic molecules is beneficial as they can fit inside the crystalline structure passivating the defects within the perovskite without causing disturbance into the lattice. [23]

Scanning electron microscopy is used to image the grains to determine whether the passivation alters the crystal size of the perovskite layer. Passivated samples are then compared to the reference sample. The scanning electron microscopy images are shown in Figure 35.

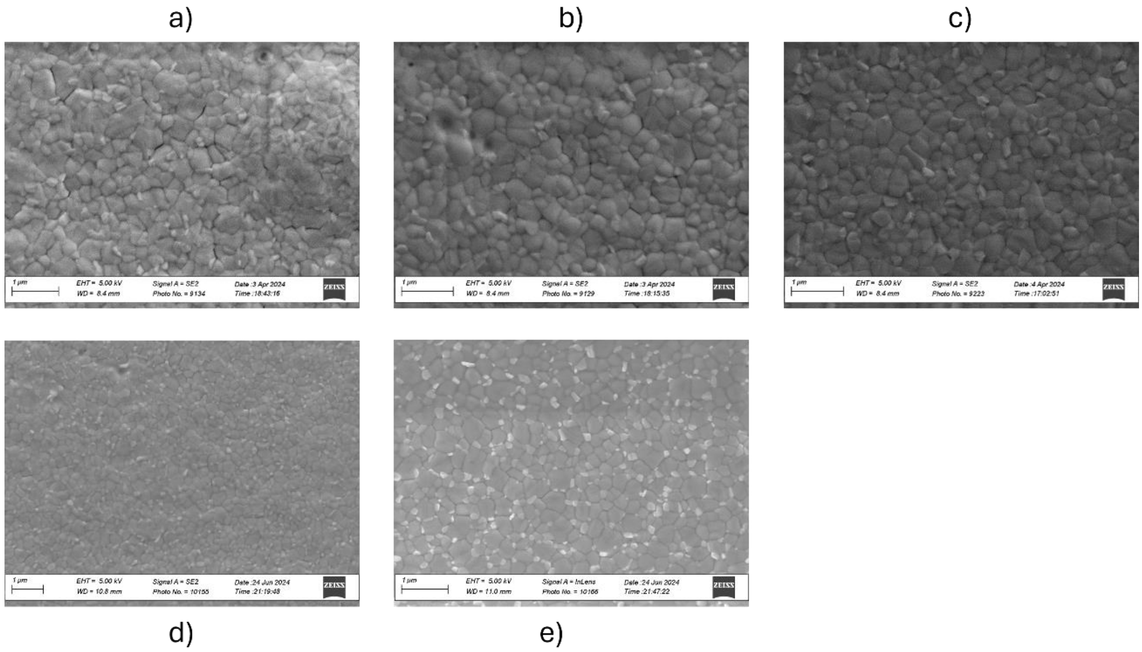

Figure 35. *Scanning electron microscopy images of the perovskite films, a) reference, b) STG 2% v/v bulk c) SHA 2% v/v bulk, d) STG 0.5 mg/ml surface and e) SHA 0.5 mg/ml surface.*

Top view SEM images of the perovskite films with and without passivation treatment are shown in Figure 35. The reference and surface passivated films show similar grain sizes, indicating that the passivated films do not have a significant effect on the morphological properties of the perovskite films. However, bulk passivated films exhibit a more uniform morphology.

To test the devices' ability to perform under stress a MPPT measurement is carried out under 1-Sun illumination, in a N2 atmosphere, and without encapsulation. In the measurement, bulk passivated devices along with a reference sample are put under constant illumination and their photovoltaic parameters are followed as a function of time. The result after 60 hours of measuring is presented in Figure 36.

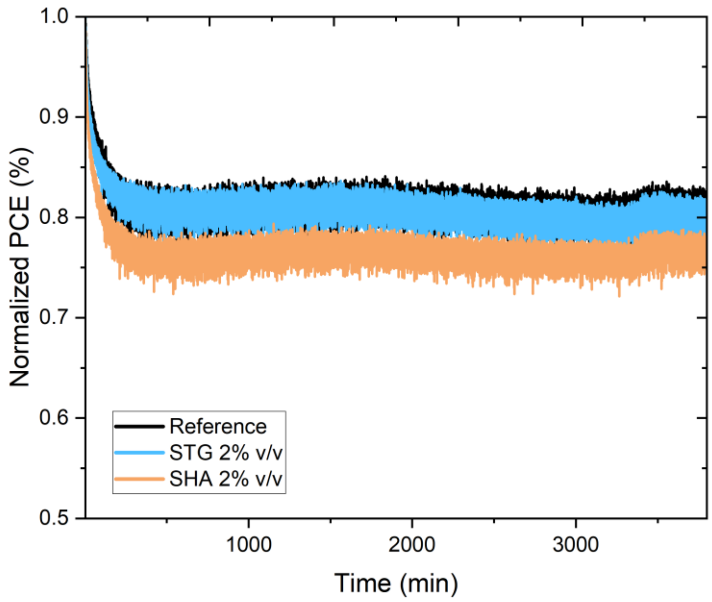

Figure 36. *Maximum power point tracking (MPPT) of devices with and without passivation.*

The bulk passivation doesn't negatively affect the performance of a perovskite solar cell under constant stress. There are no noticeable differences between the reference and passivated samples in the first two days. A longer time under illumination is needed to make proper conclusions about the stress resistance and the effect of the passivation.

The bulk passivation method was selected for additional experiments to study how the passivation affects the performance when the light intensity is decreased gradually. With this experiment the ideality factor nID can be calculated with equation

$$S = n_{ID} \frac{kT}{q} \tag{4.1}$$

where *S* is the slope of the direct fit, *k* the Boltzmann constant, *T* the temperature and *q* the elementary charge. [29] The ideality factors are calculated according to the equation 4.1. Ideality factors are presented in Figure 37 as well as the plots.

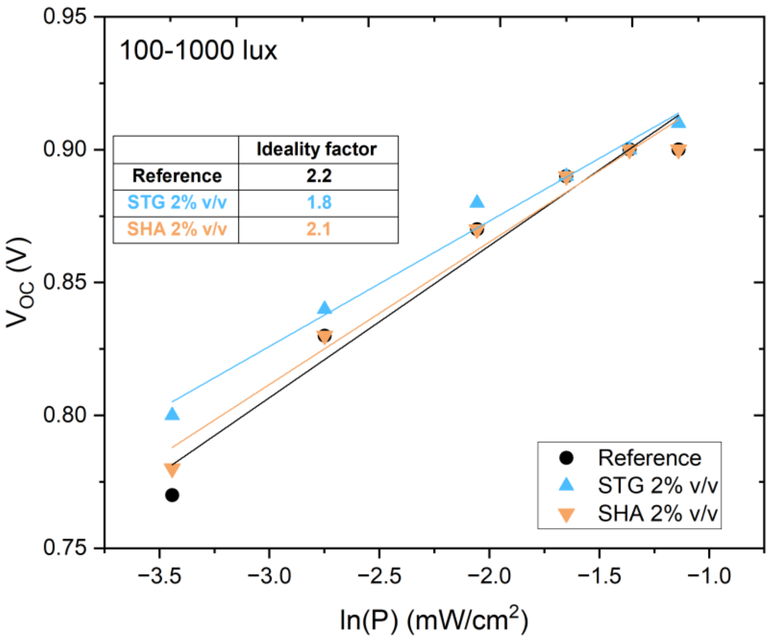

Figure 37. *The direct fit of a V_{OC} vs ln(P) plot.*

From the table in Figure 37, the ideality factors for the reference and passivated devices can be perceived. The device passivated with sodium thioglycolate STG has the lowest ideality factor of 1.8. Having ideality factor around 2 indicates that there is Shockley-Read-Hall type defect assisted recombination, which means that there are defects where the moving electrons get trapped between the energy states. The ideality factor being smaller on both passivated devices essentially means that the passivation is beneficial for the device. [18]

Shunt resistances can be obtained from the dark J-V curves of the devices. By analysing the J-V-curvature around low voltage region the shunt resistances can be obtained by taking the inverse of the fitted line. The shunt resistances for the reference and passivated devices are shown in Table 14.

Table 14. *Shunt resistances for the reference and bulk passivated devices.*

Type	Shunt resistance ($\times 10^7$ Ωcm^2)
Reference	1.12
STG 2% v/v	1.37
SHA 2% v/v	1.20

The increase in shunt resistances for passivated devices suggests that passivation enables decreased shunts inside the device, therefore improving the overall device performance. [29] Also, the effect of shunt resistance can be seen when plotting the light intensity vs. *FF* and vs. V_{OC}. The plots of bulk passivated devices plotted light intensity vs *FF* and vs V_{OC} are presented in Figure 38.

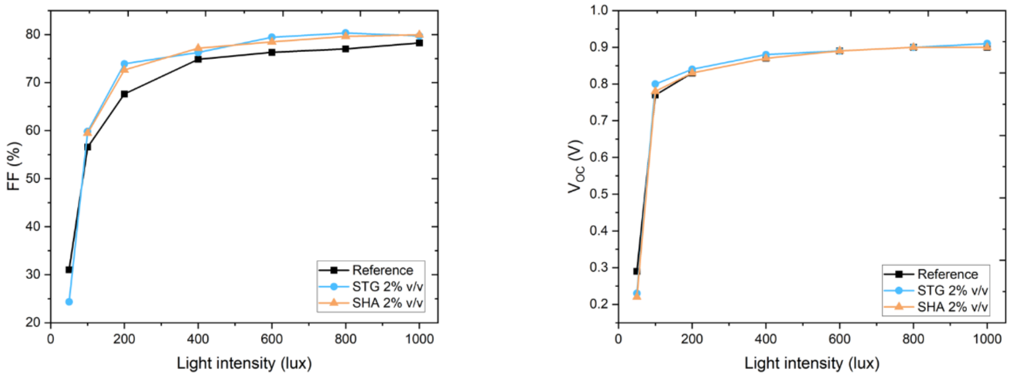

Figure 38. *Light intensity vs FF and vs* V_{OC}*.*

From both graphs, especially with *FF*, an effect of shunt resistance can be seen as the decrease in *FF* is bigger with reference sample, which indicates that the shunt resistances are significant at low light intensities. As the decrease is smaller with the passivated devices the conclusion is that the shunt resistance is increased with passivation. [29]

5. CONCLUSIONS

The goal of this thesis was to study the use of two different small organic molecules, i.e., sodium thioglycolate and sodium hydroxyacetate, in two passivation strategies, surface and bulk, to enhance the performance of perovskite-based solar cells. The first goal was to determine the most promising concentration of the passivators. The second goal was to determine the best passivation strategy. The third and final goal was to compare the molecules in the best passivation strategy into extent by characterization of the perovskite to understand the effect on passivation at a deeper level. The study was carried out by fabricating perovskite solar cells with a perovskite composition of $Cs_{0.05}(MA_{0.17}FA_{0.83})_{0.95}Pb(I_{0.83}Br_{0.17})_3$ by Saliba et al. [24] For the charge transport layers, compact TiO_2 and mesoporous TiO_2 was used as an electron transport layer, and commercial Spiro-OMeTAD as a hole transport layer. FTO and gold electrodes completed the devices structures.

By comparing the photovoltaic parameters from several device batches under 1-Sun and indoor illumination (1000 lux), the most suitable concentrations of the molecules for surface and bulk passivation were determined. For the sodium thioglycolate with surface passivation, the best concentration was 0.5 mg/ml in IPA, while for bulk passivation 2% v/v in DMSO. The results were the same for sodium hydroxyacetate.

The best passivation strategy was identified by data-analysis of the photovoltaic parameters considering the issues with solubility with surface passivation. The best bulk passivated devices performed slightly better than the reference sample under indoor illumination. Through characterization by absorbance measurements, scanning electron microscopy imaging, and X-ray diffraction analysis the effect of passivation was studied further. Absorbance measurements showed that the perovskite band gap stayed unchanged upon both passivation methods. With scanning electron imaging, the sizes of the grains on a perovskite layer resulted similar in size, thus it can be concluded that the passivation did not affect the perovskite morphology drastically. The X-ray diffraction study for bulk passivated devices showed that that the crystalline structure of perovskite was not dramatically changed upon passivation. With surface passivation, the achieved increase in V_{OC} was the highlight of the method, but the issues with surface passivation under indoor illumination hint the bulk passivation strategy is more promising for further studies. In conclusion, according to this study, the best passivation strategy with the target molecules in an *n-i-p* architecture is bulk passivation.

Third goal was to determine the champion molecule for this study. According to the obtained photovoltaic parameters, bulk passivation with sodium thioglycolate is more promising than the passivation with sodium hydroxyacetate. Nevertheless, in-depth characterization to confirm the dominance of the sodium thioglycolate must be conducted by performing additional experiments such as maximum power point tracking, light intensity dependence, and dark J-V-analysis. The bulk passivated devices were placed under a constant illumination to study their ability to withstand stress. After a time, exposure of 60 hours, there was no clear decrease in PCE of the devices. However, a longer measurement time would be needed to fully study the stress resistance and confirm whether the passivation is beneficial for the device in a long run. To understand the deep-lying effects of the bulk passivation strategy a light intensity dependence experiment was conducted for the reference and bulk passivated devices. With this experiment, the ideality factor n_{ID} was determined for reference, sodium thioglycolate, and sodium hydroxyacetate samples as 2.2, 1.8, and 2.1, respectively. Having a lower ideality factor is beneficial for the performance of the device. By studying the dark-J-V curves of the reference and bulk passivated devices also the shunt resistance can be determined. Shunt resistances for the reference, sodium thioglycolate and sodium hydroxyacetate were 1.12×10^7 Ωcm^2, 1.37×10^7 Ωcm^2 and 1.20×10^7 Ωcm^2, respectively. Bigger shunt resistance essentially means that the passivation decreases shunts within the device. By determining the ideality factor and shunt resistance, the overall superiority of the sodium thioglycolate was confirmed. For both passivation strategies, the best performing molecule was sodium thioglycolate, which also was the champion molecule in the study by Xu et al. [32]

The main findings of this study showed that the best concentration for surface passivation was 0.5 mg/ml in IPA and for bulk passivation 2% v/v in DMSO. Bulk passivation was found to be better passivation method compared to surface passivation. When comparing the two molecules, sodium thioglycolate proved to be far superior to sodium hydroxyacetate, as demonstrated by the findings of our film characterization and light intensity dependence. Reliability of the results was confirmed with external quantum efficiency measurements.

In conclusion, passivation with small bifunctional organic molecules has a lot of potential in the future. For further studies, the stress resistance of the passivation must be studied to full extent. Investigating the reasons behind the loss of short-circuit current J_{SC} and hysteresis is worthwhile, as solving it would greatly increase the PCE values of the devices. As bulk passivation enhanced the performance of the devices under indoor illumination, studying the bulk passivation strategy under low-light intensities should be continued in the future.

REFERENCES

[1] Afre, R. A., & Pugliese, D. (2024). Perovskite Solar Cells: A Review of the Latest Advances in Materials, Fabrication Techniques, and Stability Enhancement Strategies. Micromachines (Basel), 15(2), p. 1-2. https://doi.org/10.3390/mi15020192

[2] Bhattarai, S., Mhamdi, A., Hossain, I., Raoui, Y., Pandey, R., Madan, J., Bouazizi, A., Maiti, M., Gogoi, D., & Sharma, A. (2022). A detailed review of perovskite solar cells: Introduction, working principle, modelling, fabrication techniques, future challeng-es. Micro and Nanostructures, 172. https://doi.org/10.1016/j.micrna.2022.207450

[3] Bisquert, J. (2018). *The Physics of Solar Cells: Perovskites, Organics, and Photovoltaic Fundamentals* (1st ed.). CRC Press. https://doi.org/10.1201/b22380

[4] Chen, C.-Y., Jian, Z.-H., Huang, S.-H., Lee, K.-M., Kao, M.-H., Shen, C.-H., Shieh, J.-M., Wang, C.-L., Chang, C.-W., Lin, B.-Z., Lin, C.-Y., Chang, T.-K., Chi, Y., Chi, C.-Y., Wang, W.-T., Tai, Y., Lu, M.-D., Tung, Y.-L., Chou, P.-T., … Wu, C.-G. (2017). Performance Characterization of Dye-Sensitized Photovoltaics under Indoor Lighting. *The Journal of Physical Chemistry Letters*, *8*(8), 1824–1830. https://doi.org/10.1021/acs.jpclett.7b00515

[5] Cheng, W., Zhou, R., Peng, S., Wang, C., & Chen, L. (2024). Research on passivation of perovskite layer in perovskite solar cells. *Materials Today Communications*, *38*, 107879-. https://doi.org/10.1016/j.mtcomm.2023.107879

[6] Dong, C., Li, X., Ma, C., Yang, W., Cao, J., Igbari, F., Wang, Z., & Liao, L. (2021). Lycopene-Based Bionic Membrane for Stable Perovskite Photovoltaics. Advanced Functional Materials, 31(25). https://doi.org/10.1002/adfm.202011242

[7] FLUXiM. characterization techniques for organic and perovskite solar cells. (2024). URL: https://www.fluxim.com/measurement-techniques-perovskite-solar-cells#Characterization%20techniques (visited: 08/02/2024)

[8] Guo, Z., Jena, A. K., & Miyasaka, T. (2023). Halide Perovskites for Indoor Photovoltaics: The Next Possibility. ACS Energy Letters, 8(1), 90–95. https://doi.org/10.1021/acsenergylett.2c02268

[9] Honsberg, C., & Bowden, S. 2019. PVEducation – Resistive effects. URL: https://www.pveducation.org/pvcdrom/solar-cell-operation/resistive-effects (visited 08/02/2024)

[10] Li, Y., Wu, H., Qi, W., Zhou, X., Li, J., Cheng, J., Zhao, Y., Li, Y., & Zhang, X. (2020). Passivation of defects in perovskite solar cell: From a chemistry point of view. *Nano Energy*, *77*, 105237-. https://doi.org/10.1016/j.nanoen.2020.105237

[11] Lu, H., Krishna, A., Zakeeruddin, S. M., Grätzel, M., & Hagfeldt, A. (2020). Compositional and Interface Engineering of Organic-Inorganic Lead Halide Perovskite Solar Cells. *iScience*, *23*(8), 101359–101359. https://doi.org/10.1016/j.isci.2020.101359

[12] Luque, A., Hegedus, S. Handbook of Photovoltaic Science and Engineering. John Wiley & Sons Ltd, Chichester, England, 2003.

[13] Jagadamma, L. K., & Wang, S. (2021). Wide-Bandgap Halide Perovskites for Indoor Photovoltaics. Frontiers in Chemistry, 9, 632021–632021. https://doi.org/10.3389/fchem.2021.632021

[14] Makuła, P., Pacia, M., & Macyk, W. (2018). How To Correctly Determine the Band Gap Energy of Modified Semiconductor Photocatalysts Based on UV–Vis Spectra. The Journal of Physical Chemistry Letters, 9(23), 6814–6817. https://doi.org/10.1021/acs.jpclett.8b02892

[15] Mathews, I., Kantareddy, S. N., Buonassisi, T., & Peters, I. M. (2019). Technology and Market Perspective for Indoor Photovoltaic Cells. *Joule*, *3*(6), 1415–1426. https://doi.org/10.1016/j.joule.2019.03.026

[16] Mertens, R. Perovskite-Info. The advantages of perovskite solar technology. (2023). URL: https://www.perovskite-info.com/advantages-perovskite-solar-technology (visited: 08/17/2024)

[17] Miah, Md. H., Khandaker, M. U., Rahman, Md. B., Nur-E-Alam, M., & Islam, M. A. (2024). Band gap tuning of perovskite solar cells for enhancing the efficiency and stability: issues and prospects. RSC Advances, 14(23), 15876–1596. https://doi.org/10.1039/d4ra01640h

[18] Miyasaka, T. (2022). *Perovskite Photovoltaics and Optoelectronics: From Fundamentals to Advanced Applications* (1st ed.). John Wiley & Sons, Incorporated. https://doi.org/10.1002/9783527826391

[19] Ochoa-Martinez, E., Ochoa, M., Ortuso, R. D., Ferdowsi, P., Carron, R., Tiwari, A. N., Steiner, U., & Saliba, M. (2021). Physical Passivation of Grain Boundaries and Defects in Perovskite Solar Cells by an Isolating Thin Polymer. ACS Energy Letters, 6(7), 2626–2634. https://doi.org/10.1021/acsenergylett.1c01187

[20] Ossila. Spiro-OMeTAD. (2024). https://www.ossila.com/products/spiro-ometad (visited 08/21/2024)

[21] P. Mäkinen. Fluorene-based hole transport materials for halide perovskite solar cells. eng. Available: https://urn.fi/URN:NBN:fi:tuni-202111158425. Faculty of Engineering and Natural Sciences, 2021.

[22] Peplow, M. (2023). ARE PEROVSKITES THE FUTURE OF SOLAR POWER? *Nature (London)*, *623*(7989), 902–905. https://doi.org/10.1038/d41586-023-03714-y

[23] Pica, G., Montecucco, R., Zanetta, A., Oranskaia, A., Faini, F., Pancini, L., Mrkyvkova, N., Siffalovic, P., Dally, P., Pirota, V., Ledinsky, M., De Bastiani, M., De Wolf, S., Doria, F., Schwingenschlögl, U., & Grancini, G. (2024). Unraveling Bulk versus Surface Passivation Effects in Highly Efficient p–i–n Perovskite Solar Cells Using Thiophene-Based Cations. Solar RRL, 8(9). https://doi.org/10.1002/solr.202300681

[24] Saliba, M., Matsui, T., Seo, J. Y., Domanski, K., Correa-Baena, J. P., Nazeeruddin, M. K., Zakeeruddin, S. M., Tress, W., Abate, A., Hagfeldt, A., & Grätzel, M. (2016). Cesium-containing triple cation perovskite solar cells: Improved stability, reproducibility and high efficiency. Energy & Environmental Science, 9(6), 1989–1997. https://doi.org/10.1039/c5ee03874j

[25] Siekmann, J., Kulkarni, A., Akel, S., Klingebiel, B., Saliba, M., Rau, U., & Kirchartz, T. (2023). Characterizing the Influence of Charge Extraction Layers on the Performance of Triple-Cation Perovskite Solar Cells. Advanced Energy Materials, 13(32). https://doi.org/10.1002/aenm.202300448

[26] SolarPower Europe. A solar lifeline in times of Energy Crisis. (2024). URL: https://www.solarpowereurope.org/advocacy/energy-crisis (visited: 17/8/2024)

[27] Srivishnu, K. S., Rajesh, M. N., Prasanthkumar, S., & Giribabu, L. (2023). Photovoltaics for indoor applications: Progress, challenges and perspectives. *Solar Energy*, *264*, 112057-. https://doi.org/10.1016/j.solener.2023.112057

[28] Thankappan, A., & Thomas, S. (2018). *Perovskite Photovoltaics - Basic to Advanced Concepts and Implementation* (1st ed.). Elsevier. https://doi.org/10.1016/C2016-0-03790-7

[29] These, A., Koster, L. J. A., Brabec, C. J., & Le Corre, V. M. (2024). Beginner's Guide to Visual Analysis of Perovskite and Organic Solar Cell Current Density–Voltage Characteristics. *Advanced Energy Materials*, *14*(21). https://doi.org/10.1002/aenm.202400055

[30] Tiwari, G. N., Tiwari, A., & Shyam. (2016). *Handbook of Solar Energy : Theory, Analysis and Applications* (1st ed. 2016.). Springer Singapore. https://doi.org/10.1007/978-981-10-0807-8

[31] Wang, Haifei et al. "Recent Progress in Large-Area Perovskite Photovoltaic Modules." *Transactions of Tianjin University* 28.5 (2022): 323–340. Web.

[32] Xu, J., Chen, H., Grater, L., Liu, C., Yang, Y., Teale, S., Maxwell, A., Mahesh, S., Wan, H., Chang, Y., Chen, B., Rehl, B., Park, S. M., Kanatzidis, M. G., & Sargent, E. H. (2023). Anion optimization for bifunctional surface passivation in perovskite solar cells. Nature Materials, 22(12), 1507–1514. https://doi.org/10.1038/s41563-023-01705-y

[33] Yang, B., Suo, J., Di Giacomo, F., Olthof, S., Bogachuk, D., Kim, Y., Sun, X., Wagner, L., Fu, F., Zakeeruddin, S. M., Hinsch, A., Grätzel, M., Di Carlo, A., & Hagfeldt, A. (2021). Interfacial Passivation Engineering of Perovskite Solar Cells with Fill Factor over 82% and Outstanding Operational Stability on n-i-p Architecture. ACS Energy Letters, 6(11), 3916–3923. https://doi.org/10.1021/acsenergylett.1c01811

[34] Yu, Y., Xia, J., & Liang, Y. (2022). Basic understanding of perovskite solar cells and passivation mechanism. *AIP Advances*, *12*(5), 055307-055307–055318. https://doi.org/10.1063/5.0058441

[35] Zhang, Zhihao et al. “Rationalization of Passivation Strategies toward High-Performance Perovskite Solar Cells.” *Chemical Society reviews* 52.1 (2023): 163–195. Web

[36] Zhao, P., Kim, B. J., & Jung, H. S. (2018). Passivation in perovskite solar cells: A review. *Materials Today Energy*, *7*, 267–286. https://doi.org/10.1016/j.mtener.2018.01.004

[37] Zimmermann, E., Ehrenreich, P., Pfadler, T., Dorman, J. A., Weickert, J., & Schmidt-mende, L. (2014). Erroneous efficiency reports harm organic solar cell research. Nature Photonics, 8(9), 669-. https://doi.org/10.1038/nphoton.2014.210